ACS OMEGA

Article

http://pubs.acs.org/journal/acsodf

N,N′-Dialkylcystine Gemini and Monomeric *N*-Alkyl Cysteine Surfactants as Corrosion Inhibitors on Mild Steel Corrosion in 1 M HCl Solution: A Comparative Study

Ruby Aslam,[†] Mohammad Mobin,*[,†] Saman Zehra,[†] Ime B. Obot,[‡] and Eno E. Ebenso[§]

[†]Corrosion Research Laboratory, Department of Applied Chemistry, Faculty of Engineering and Technology, Aligarh Muslim University, Aligarh 202002, India

[‡]Centre of Research Excellence in Corrosion, Research Institute, King Fahd University of Petroleum and Minerals, Dhahran 31261, Saudi Arabia

[§]Material Science Innovation & Modelling (MaSIM) Research Focus Area, Faculty of Agriculture, Science and Technology, North-West University (Mafikeng Campus), Private Bag X2046, Mmabatho 2735, South Africa

Supporting Information

ABSTRACT: Gemini surfactant, *N,N′*-dialkylcystine 2-(C_{12}Cys), derived from cystine, and a monomeric *N*-alkyl cysteine counterpart, (C_{12}Cys), were synthesized and purified. The characterization of surfactants 2(C_{12}Cys) and (C_{12}Cys) was made by Fourier transform infrared, ^{1}H NMR, and elemental analysis. The effect of 2(C_{12}Cys) and (C_{12}Cys) on mild steel (MS) corrosion in 1 M HCl solution was explored as a function of their concentration and electrolyte temperature by means of gravimetric and electrochemical experiments (potentiodynamic polarization and Electrochemical impedance spectroscopy), surface analytical techniques (scanning electron microscopy (SEM)/energy dispersive X-ray spectroscopy (EDAX) and atomic force microscopy (AFM)) and theoretical study. The investigated compounds exhibited surface active properties and performed as good inhibitors for corrosion control of mild steel (MS) in acid solution. However, compared to monomeric (C_{12}Cys), Gemini surfactant 2(C_{12}Cys) showed high corrosion inhibiting ability at very low concentration. The EIS results revealed a greater charge transfer resistance in 2(C_{12}Cys) solution compared to that in (C_{12}Cys) solution. SEM/EDAX observations validate the development of an inhibitive film by the adsorbed molecules of surfactant on the MS surface. The AFM micrographs supported the SEM/EDAX results and exhibited a lowering in the roughness of the corroded MS surface in the presence of both (C_{12}Cys) and 2(C_{12}Cys) surfactants. Further, quantum chemical calculations and Monte Carlo simulations were used to study the dependence of corrosion inhibiting efficacy on the molecular structure and adsorption strength.

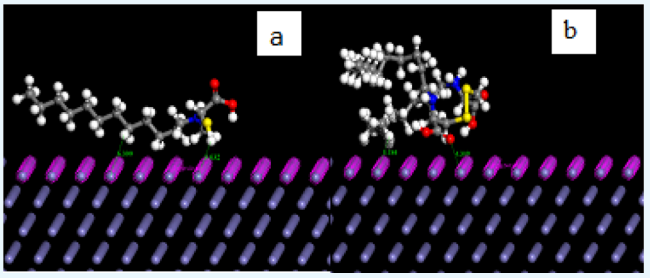

1. INTRODUCTION

Mild steel (MS) is highly utilized in various industrial fields such as petro-chemical, oil and gas, nuclear, pulp and paper, power, and desalination. This is attributable to its high strength, malleability, low cost, and affordability.[1−3] Owing to the above-mentioned properties, there is a desire to maximize the lifetimes of MS items, with one of the prime causes of degradation being corrosion, specifically in aggressive acidic environments.[4,5] Acids like HCl and H_2SO_4 are used to pickle steel, where impurities like stains, rust, or scales are detached from the surface.[6−8] Despite it being more costly than H_2SO_4, HCl pickles at a much faster speed, thereby reducing corrosion loss of the base metal. To control base metal corrosion, various approaches are used, with inhibitors being one of the cheapest and most familiar methods.[9−11] Compounds having heteroatoms like nitrogen, sulfur, and oxygen with high electron density have been found to be potential inhibitors against metal corrosion in many environments.[12−15] But, a number of them are very harmful and raise environmental concerns. Currently, the principal objective in selecting compounds to inhibit corrosion for practical application apart from efficiency is their eco-friendliness due to the issues of environmental pollution.

Among the class of compounds employed as corrosion inhibitors, surfactants have the advantages of good inhibition efficiency, being safe and easy to use, and economical production.[16,17] The hydrophilic part of the molecules of surfactants facilitates their aggregation and adsorption on metallic surfaces thus blocking active sites on the surfaces and thereby protecting them from corrosion.[18,19] Furthermore, molecules of surfactants tend to avoid the polar aqueous phase by associating and aggregating their hydrophobic hydrocarbon chains together.[20]

Among the surfactants, Gemini surfactants (double chain) have attracted the attention of the scientific community because

Received: April 24, 2017
Accepted: August 29, 2017
Published: September 11, 2017

DOI: 10.1021/acsomega.7b00501
ACS Omega 2017, 2, 5691−5707

of their better aggregation properties than those of traditional single chain surfactants.[21,22] Gemini surfactants obtained from amino acids have attracted significant interest in the recent past as they are reported to be biocompatible and biodegradable surfactants that fulfill the requirements of biological and ecological compatibility[23,24] with enhanced performance for biomedical and technological implementation.

In this work, we provide a complete view of the Gemini surfactant based on the amino acid cystine,[25] which is designated as 2(C_{12}Cys), where C represent the number of C atoms in the hydrophobic chain moiety, from the viewpoint of synthesis and corrosion protection performance, and compare to a cysteine-based monomeric surfactant, which is designated as (C_{12}Cys). Cysteine is an α-amino acid, which contains not only carboxyl [−COOH] and amino [$-NH_2$] functional groups, but also a [−SH] group. It has the capability to control corrosion by coordinating with metals through the N atom, O atom of the carboxyl group, and S atom of the thiol group, which could explain the interest of this molecule as a potential inhibitor for MS. The novelty in the current study stems from the fact that Yoshimura et al.[25] only investigated the adsorption and aggregation properties of these compounds, whereas for the first time in the literature, we have established the anticorrosive properties of these compounds in the corrosion of MS in acid solution employing advanced experimental techniques and theoretical calculations. The anticorrosion performance was investigated by gravimetric measurements, electrochemical measurements (potentiodynamic polarization (PDP) and electrochemical impedance spectroscopy (EIS)), and surface assessment techniques (scanning electron microscopy (SEM)/energy dispersive X-ray spectroscopy (EDAX) and atomic force microscopy (AFM)). The anticorrosion performances of 2(C_{12}Cys) and (C_{12}Cys) are correlated with quantum chemical parameters and Monte Carlo simulations in expectation that the interrelationship will be assistive in the design and synthesis of new inhibitors with higher inhibition efficiency.

2. RESULTS AND DISCUSSION

2.1. Critical Micelle Concentration (CMC) Determination. CMC values of 2(C_{12}Cys) and (C_{12}Cys) were obtained in 1 M HCl aqueous solution from the change in the slope of the plotted data of γ versus the solute concentration (log C), see Figure S1, (Supporting Information). To get further insight into the interfacial adsorption of (C_{12}Cys) or 2(C_{12}Cys), CMC values along with other interfacial parameters such as effectiveness (π_{CMC}),[25] maximum surface excess (Γ_{max}),[26] minimum surface area (A_{min}),[27] standard free energy of micellization (ΔG°_{mic}), and standard free energy of adsorption (ΔG°_{ads})[29,30] at the air/solution interface were computed from the surface tension profiles of the evaluated surfactants, and the results are given in Table S1 (Supporting Information). 2(C_{12}Cys) was observed to be more efficient because it attained the maximum reduction in γ at CMC. A large value of Γ_{max} implies the adsorption of more surfactant molecules on the solution surface, which also means a lowering in surface tension. A low A_{min} value[28] suggests tight packing or complete surface coverage at the interface by the prepared surfactants. The reduction of surface tension and A_{min} value of 2(C_{12}Cys) indicate that this compound acts as an effective corrosion inhibitor for MS in 1 M HCl solution. Negative values of ΔG°_{mic} and ΔG°_{ads} reflect that both processes are spontaneous. Spontaneity in the 2(C_{12}Cys) system is more remarkable than that in (C_{12}Cys). Additionally, the ΔG°_{ads} and ΔG°_{mic} values are near to each other with slightly more negativity of ΔG°_{ads}, implying that the adsorption of 2(C_{12}Cys) or (C_{12}Cys) at the interface is preferable.[31]

2.2. Open-Circuit Potential (OCP)−Time Curves. Prior to commencement of an electrochemical (PDP and EIS) experiment a steady-state potential was established. The representative experimental variation of the open-circuit potential (E_{OCP}) with time, measured in 1 M HCl with different (C_{12}Cys) concentrations at 303 K, is presented in Figure S2 (Supporting Information). It took approximately 800 s to reach a stable OCP value.

2.3. Potentiodynamic Polarization Measurements (PDP). Representative PDP (anodic and cathodic polarization) curves of MS in 1 M HCl solutions without and with different concentrations of 2(C_{12}Cys) are presented in Figure 1, and the

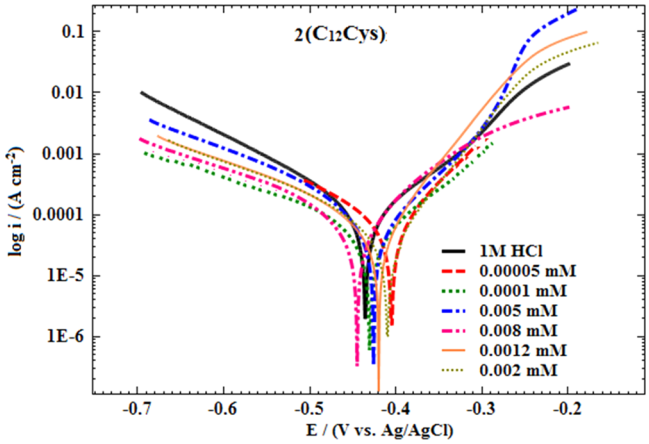

Figure 1. Potentiodynamic polarization curves for MS in 1 M HCl containing different concentrations of 2(C_{12}Cys) (temperature 303 ± 2 K).

corresponding polarization parameters obtained by the extrapolation of the linear segments of the anodic and cathodic curves are listed in Table 1. The polarization curves show that the presence of (C_{12}Cys) or 2(C_{12}Cys) decreased both the anodic and cathodic current densities, decreasing the corrosion current density (I_{corr}).

The decrease in I_{corr} is more evident with increasing (C_{12}Cys) or 2(C_{12}Cys) concentration compared to the uninhibited solution. In the present article, the shift in the values of E_{corr} of the inhibited systems in relation to the uninhibited solution is <85 mV. The values of E_{corr} tend to change toward the positive direction, implying the presence of (C_{12}Cys) or 2(C_{12}Cys) inhibited oxidation of Fe and decreased hydrogen evolution, implying that both studied compounds act as mix-type corrosion inhibitors with a predominating anodic character. Table 1 shows that the values of I_{corr} of the acid solutions containing (C_{12}Cys) or 2(C_{12}Cys) are significantly smaller compared to that of the uninhibited acid solution, implying that the acid corrosion of MS is effectively hindered by both inhibitors. The values of I_{corr} of the lowest studied concentration of (C_{12}Cys) (1×10^{-3} mM) and 2(C_{12}Cys) (5×10^{-5} mM) are 0.48×10^{-4} and 0.67×10^{-4} A cm^{-2}, respectively, corresponding to inhibition efficiency (η_{PDP}, %) values of 65.3 and 51.9%. There is a progressive lowering in the I_{corr} values with increasing (C_{12}Cys) and 2(C_{12}Cys) concentration.

When the concentration was increased from 1×10^{-3} to 0.2 mM (C_{12}Cys) and 5×10^{-5} to 2×10^{-3} mM 2(C_{12}Cys), the I_{corr} values changed to 0.17×10^{-4} and 0.31×10^{-4} A cm^{-2}, and the

DOI: 10.1021/acsomega.7b00501
ACS Omega 2017, 2, 5691−5707

Table 1. PDP Parameters for MS in 1 M HCl in the Absence and Presence of Different Concentrations of (C_{12}Cys) and 2(C_{12}Cys)[a]

inhibitor	C_{inh} (mM)	E_{corr} (V vs Ag/AgCl)	β_a (V dec^{-1})	β_c (V dec^{-1})	$I_{corr} \times 10^{-4}$ (A cm^{-2})	η_{PDP} (%)
blank	0	−0.436	0.137	0.135	1.4 ± 0.09	
(C_{12}Cys)	1×10^{-3}	−0.443	0.103	0.074	0.48 ± 0.04	65.3
	7×10^{-3}	−0.420	0.087	0.052	0.35 ± 0.01	74.4
	1×10^{-2}	−0.414	0.111	0.088	0.27 ± 0.03	78.7
	7×10^{-2}	−0.421	0.086	0.091	0.24 ± 0.03	81.3
	0.15	−0.417	0.062	0.063	0.19 ± 0.02	85.6
	0.2	−0.435	0.043	0.056	0.17 ± 0.05	86.5
2(C_{12}Cys)	5×10^{-5}	−0.406	0.126	0.073	0.67 ± 0.07	51.9
	1×10^{-4}	−0.433	0.148	0.115	0.58 ± 0.05	54.9
	5×10^{-4}	−0.425	0.089	0.081	0.54 ± 0.02	58.1
	8×10^{-4}	−0.443	0.103	0.074	0.41 ± 0.03	68.3
	1.2×10^{-3}	−0.420	0.087	0.052	0.35 ± 0.04	72.6
	2×10^{-3}	−0.413	0.092	0.057	0.31 ± 0.01	75.8

[a]Temperature 303 ± 2 K.

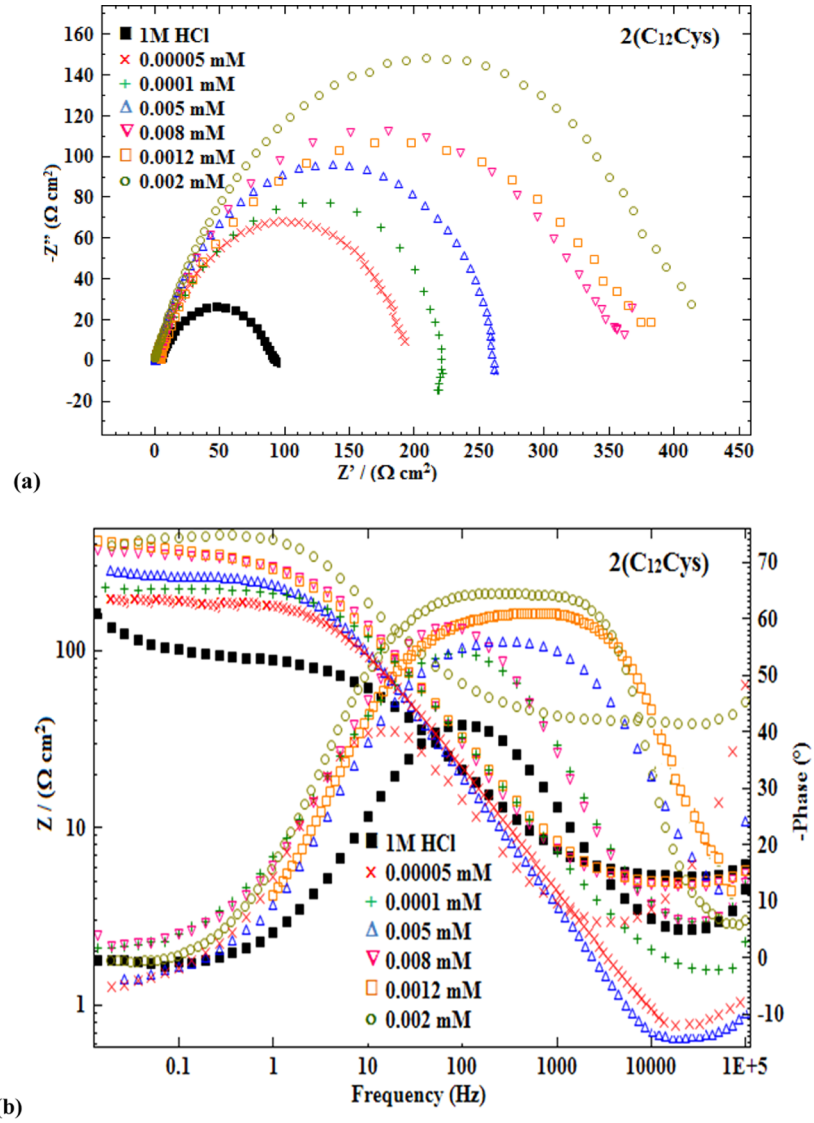

Figure 2. (a) Nyquist plots and (b) Bode plots for MS in 1 M HCl containing various concentrations of 2(C_{12}Cys).

inhibition efficiency increased to 86.5 and 75.8%, respectively. This suggests that in the presence of the inhibitors (C_{12}Cys) or 2(C_{12}Cys), a protective layer is formed on the MS surface, which acts as a barrier between MS and the HCl solution; this resulted in the retardation of electrochemical reactions at the electrode surface.

The variation of the Tafel slopes with inhibitor concentration does not follow a definite trend, indicating that the studied

DOI: 10.1021/acsomega.7b00501
ACS Omega 2017, 2, 5691−5707

Table 2. EIS Parameters for MS in 1 M HCl Containing Different Concentrations of (C_{12}Cys) and 2(C_{12}Cys)[a]

				CPE			
inhibitor	C_{inh} (mM)	R_s (Ω cm^2)	R_{ct} (Ω cm^2)	$Y_o \times 10^{-4}$ (Ω^{-1} s^n cm^{-2})	n	$C_{dl} \times 10^{-4}$ (μF cm^{-2})	η_{EIS} (%)
blank	0	4.64	91.7 ± 5.50	1.51	0.9940	1.36	
(C_{12}Cys)	1×10^{-3}	1.16	266.8 ± 9.60	1.64	0.9964	1.62	65.6
	7×10^{-3}	4.84	342.0 ± 5.47	1.18	0.9955	1.15	73.2
	1×10^{-2}	2.04	418.1 ± 11.95	0.89	0.9963	0.88	78.1
	7×10^{-2}	5.36	443.1 ± 25.96	0.83	0.9969	0.82	79.3
	0.15	1.01	616.3 ± 22.18	0.73	0.9955	0.71	85.1
	0.2	8.26	752.9 ± 34.63	0.68	0.9944	0.67	87.8
(C_{12}Cys)$_2$	5×10^{-5}	0.93	196.5 ± 9.82	1.12	0.9959	1.11	53.3
	1×10^{-4}	2.60	224.6 ± 12.12	1.10	0.9959	1.08	59.1
	5×10^{-4}	1.16	266.7 ± 10.20	0.91	0.9964	0.90	65.6
	8×10^{-4}	4.84	342.0 ± 8.20	0.81	0.9955	0.80	73.2
	1.2×10^{-3}	3.91	373.5 ± 16.80	0.71	0.9941	0.70	76.1
	2×10^{-3}	2.58	414.5 ± 4.35	0.61	0.9962	0.60	77.8

[a]Temperature 303 ± 2 K.

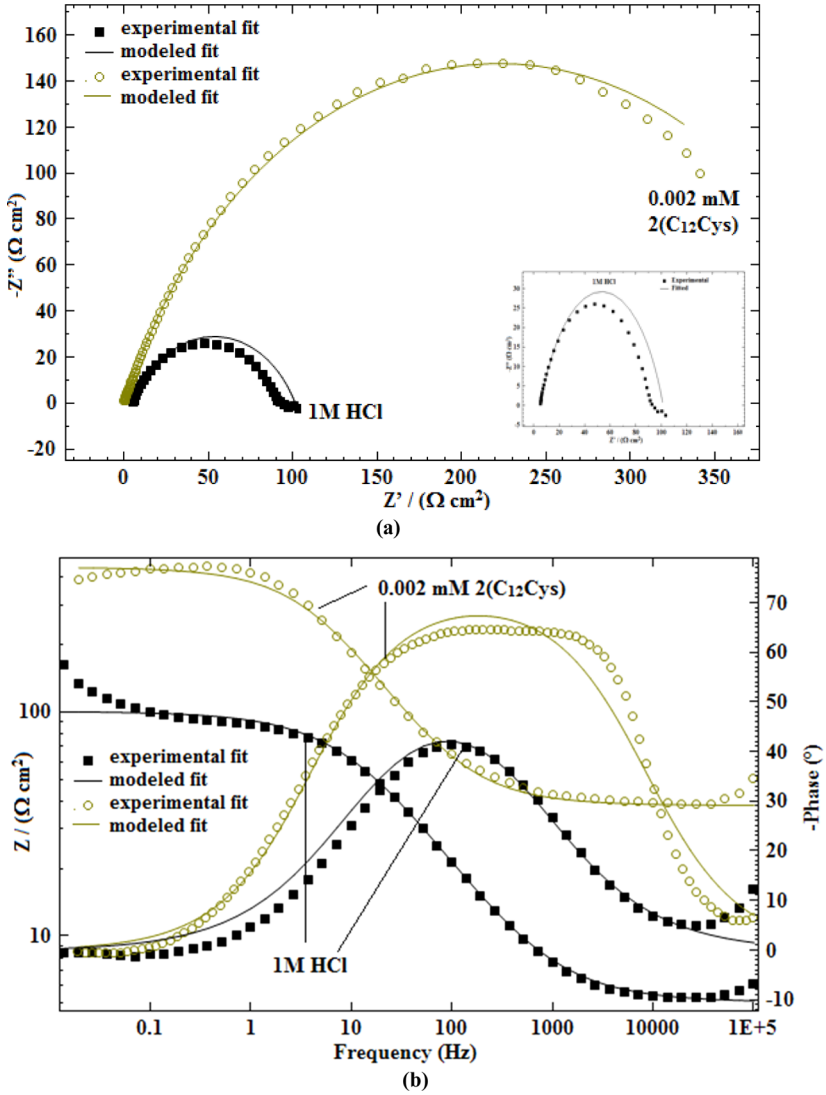

Figure 3. Experimental and computer fit results: (a) Nyquist plots; (b) Bode plots.

surfactants insignificantly affected either the anodic iron dissolution or cathodic hydrogen evolution, and rather, inhibition occurred by a blocking mechanism on the available metal spaces.[32] The η_{PDP} (%) of (C_{12}Cys) and 2(C_{12}Cys) obtained from corrosion current densities shows that efficiency is proportional to inhibitor concentration. However, 2(C_{12}Cys) showed quite high inhibition efficiency at minimal concentration in comparison to (C_{12}Cys).

DOI: 10.1021/acsomega.7b00501
ACS Omega 2017, 2, 5691−5707

2.4. Electrochemical Impedance Spectroscopy (EIS). Representative impedance spectra obtained without and with different concentrations of 2(C_{12}Cys) in 1 M HCl are presented in Figure 2. Impedance parameters (Table 2) were obtained utilizing the application of the equivalent circuit model.

Simplest fitting is represented by the Randles equivalent circuit (Figure S3, Supporting Information). This circuit is a parallel combination of R_{ct} (charge transfer resistance) and C_{dl} (double layer capacitance), both in series with R_s (the solution resistance). It is evident from Figure 2a that all of the obtained impedance spectra exhibited a single capacitive loop, which suggests that the corrosion of MS in both uninhibited and inhibited 1 M HCl is usually associated with double layer behavior[33] and mostly controlled by a charge transfer process under the open-circuit conditions. Moreover, for all of the evaluated concentrations, the impedance spectra have identical shape, implying that addition of 2(C_{12}Cys) or (C_{12}Cys) into the corrosive solution does not cause a change in the corrosion mechanism. The occurrence of depressed semicircles is proposed to be due to the frequency dispersion of interfacial impedance.[34] This capacitance dispersion at the metal surfaces is mainly due to surface roughness, the chemical heterogeneity of the surface, and the adsorption−desorption process of inhibitor molecules on the MS surface.[35]

To overcome this situation, a constant phase element (CPE) that corresponds to surface roughness, impurities, degree of polycrystallinity, chemical inhomogeneities, and adsorption of inhibitive molecules[36] is introduced in the equivalent circuit in place of C_{dl}. CPE, the impedance function, is given as follows.[36]

$$Z_{CPE} = \frac{1}{Y_0(j\omega)^n} \quad (1)$$

where Y_0 is the CPE constant, j is the imaginary unit, ω is the angular frequency, and n is the CPE exponent (represents the deviation from the ideal performance and it ranges between 0 and 1). The lower value of n (Table 2) for MS in the studied corrosive solution indicates surface irregularity resulting from MS surface roughening due to corrosion.

However, in (C_{12}Cys) or 2(C_{12}Cys) inhibited solutions, n values were observed to increase, indicating a reduction in inhomogeneity of the surface due to the adsorption of inhibitor molecules.[37] Y_0 is converted into C_{dl} by the use of the following equation.[34]

$$C_{dl} = Y_0(\omega_{max})^{n-1} \quad (2)$$

where $\omega_{max} = 2\pi f_{max}$ (f_{max} denotes maximum frequency at which the imaginary component of the impedance has a maximum). The experimental and computer fit results of the Nyquist plots and Bode plots (impedance and θ) for MS in 1 M HCl and 1 M HCl containing 2×10^{-3} mM of 2(C_{12}Cys) are shown in Figure 3a,b. It can be seen that the fit results are agreeable with the experimental data within 10% error. The inset figure (Figure 3a) depicts the magnified form of the Nyquist plots for the blank.

From the impedance data given in Table 2, it is clear that the values of R_{ct} for the (C_{12}Cys) or 2(C_{12}Cys) inhibited solutions rises with the concentration of the inhibitors. This is related to the formation of a protective layer at the MS−acid interface. The C_{dl} values are observed to decrease with an increase in concentration of (C_{12}Cys) or 2(C_{12}Cys). The lowering in C_{dl} value for the inhibited solutions is attributed to the increase in the electrical double layer thickness and/or a drop in the local dielectric constant.[37] Further, the decrease in the C_{dl} values verifies the adsorption of (C_{12}Cys) or 2(C_{12}Cys) molecules on the MS surface by replacing water molecules, leading to a reduction in the number of active sites available for the corrosion reaction. Also, the increase of R_{ct} values with increasing surfactant concentration indicates that the charge transfer process is mainly controlling the corrosion process. In contrast, the better protection given by an inhibitor can be associated with a decrease in the capacitance of the metal. Typically, at 1×10^{-3} mM of each inhibitor, the presence of (C_{12}Cys) gives an R_{ct} value of 266.8 (Ω cm^2) and C_{dl} value of 1.62×10^{-4} (μF cm^{-2}), whereas 2(C_{12}Cys) gives respective values of 373.5 (Ω cm^2) and 0.70×10^{-4} (μF cm^{-2}), respectively. This implies the improved inhibition by 2(C_{12}Cys) over that of (C_{12}Cys). The values of inhibition efficiency (η_{EIS}) were calculated from R_{ct} in the absence and presence of the inhibitors. In both cases, η_{EIS} increases with the inhibitor concentrations, and follows the order: η_{EIS} 2(C_{12}Cys) > η_{EIS} (C_{12}Cys), in accordance with the results from the potentiodynamic polarization measurements.

Bode plots for MS immersed in 1 M HCl containing various concentrations of (C_{12}Cys) or 2(C_{12}Cys) inhibitor exhibit one time constant. This show that the (C_{12}Cys) or 2(C_{12}Cys) systems form a monolayer and the charge transfer reaction controls the dissolution process occurring at the MS/solution interface.[38] As we can see in Figure 2b, raising the concentration of surfactant (C_{12}Cys) or 2(C_{12}Cys) in the HCl solution results in a phase angle closer to 90°, suggesting excellent inhibitive behavior due to adsorption of more (C_{12}Cys) or 2(C_{12}Cys) molecules on the MS surface at higher concentrations. Further, the shift of phase angle for the inhibited systems suggests a change in the electrode interfacial structure upon addition of (C_{12}Cys) or 2(C_{12}Cys). The regular increase in the phase angle shift in the inhibited solution is obviously associated with the growth of the inhibitor film and increased surface coverage on the MS surface, resulting in a higher inhibition efficiency. Considering the frequency versus impedance plots (see Figure 2b), the impedance values for the 2(C_{12}Cys) or (C_{12}Cys) inhibited systems is higher than that in their absence. Further, the value of impedance increased with increasing surfactant concentration, suggesting the corrosion rate of MS in HCl solution is decreased by the addition of (C_{12}Cys) or 2(C_{12}Cys), and continues to decrease on increasing the concentration of the surfactants.

2.5. Gravimetric Measurement. *2.5.1. Influence of Concentration and Immersion Time on Corrosion Inhibition.* The inhibition efficiency (η_w) values calculated from weight loss measurements for MS in 1 M HCl solution having various concentrations of (C_{12}Cys) or 2(C_{12}Cys) inhibitors at the four temperatures 303, 313, 323, and 333 K are given in Table 3. It is apparent from the table that the studied inhibitors reduced the corrosion of MS in acid medium markedly. η_w increased with an enhancement in the concentration of the studied inhibitors and reached a maximum at 0.2 and 2×10^{-3} mM of (C_{12}Cys) and 2(C_{12}Cys), respectively. The increase in η_w with increasing inhibitor concentration is suggestive of the enhancement in the degree of adsorption of (C_{12}Cys) or 2(C_{12}Cys) on the MS surface.

The η_w (%) of (C_{12}Cys) and 2(C_{12}Cys) was found to be 86.5 and 73.4%, respectively, at 0.2 and 2×10^{-3} mM at 303 K. The η_w (%) of (C_{12}Cys) and 2(C_{12}Cys) over the range of concentrations studied is higher than that reported for some monomeric and Gemini surfactants in the literature[39−48] (see Table 4). Compared to previously studied monomeric and Gemini surfactants based corrosion inhibitors, the present compound

DOI: 10.1021/acsomega.7b00501
ACS Omega 2017, 2, 5691−5707

Table 3. Corrosion Parameters Obtained from Weight Loss Measurements for MS in 1 M HCl Containing Various (C_{12}Cys) and 2(C_{12}Cys) Concentrations after 6 h Immersion at Temperatures of 303−333 K

		303 K			313 K			323 K			333 K		
inhibitor	C_{inh} (mM)	ν_w (mg cm^{-2} h^{-1})	θ	η_w (%)	ν_w (mg cm^{-2} h^{-1})	θ	η_w (%)	ν_w (mg cm^{-2} h^{-1})	θ	η_w (%)	ν_w (mg cm^{-2} h^{-1})	θ	η_w (%)
0		0.137 ± 0.003			0.387 ± 0.009			2.205 ± 0.055			7.117 ± 0.557		
(C_{12}Cys)	1×10^{-3}	0.052 ± 0.001	0.617	61.7	0.124 ± 0.005	0.679	67.9	0.646 ± 0.008	0.704	70.4	1.825 ± 0.091	0.743	74.3
	7×10^{-3}	0.036 ± 0.001	0.736	73.6	0.088 ± 0.003	0.774	77.4	0.433 ± 0.006	0.802	80.2	1.186 ± 0.043	0.832	83.2
	1×10^{-2}	0.029 ± 0.001	0.787	78.7	0.073 ± 0.004	0.814	81.4	0.304 ± 0.009	0.864	86.4	0.776 ± 0.045	0.891	89.1
	7×10^{-2}	0.026 ± 0.001	0.812	81.2	0.059 ± 0.003	0.846	84.6	0.344 ± 0.007	0.892	89.2	0.547 ± 0.027	0.920	92.0
	0.15	0.021 ± 0.001	0.845	84.5	0.049 ± 0.001	0.872	87.2	0.184 ± 0.008	0.916	91.6	0.38 ± 0.015	0.947	94.7
	0.2	0.018 ± 0.001	0.865	86.5	0.041 ± 0.002	0.891	89.1	0.167 ± 0.003	0.928	92.8	0.348 ± 0.020	0.951	95.1
2(C_{12}Cys)	5×10^{-5}	0.073 ± 0.003	0.465	46.5	0.223 ± 0.01	0.428	42.8	1.109 ± 0.014	0.492	49.2	3.064 ± 0.153	0.568	56.8
	1×10^{-4}	0.063 ± 0.002	0.543	54.3	0.16 ± 0.01	0.587	58.7	0.85 ± 0.016	0.613	61.3	2.281 ± 0.084	0.679	67.9
	5×10^{-4}	0.053 ± 0.002	0.613	61.3	0.125 ± 0.01	0.679	67.9	0.669 ± 0.013	0.697	69.7	1.658 ± 0.098	0.767	76.7
	8×10^{-4}	0.046 ± 0.002	0.664	66.4	0.095 ± 0.005	0.754	75.4	0.494 ± 0.013	0.778	77.8	0.958 ± 0.048	0.865	86.5
	1.2×10^{-3}	0.038 ± 0.002	0.721	72.1	0.079 ± 0.002	0.796	79.6	0.421 ± 0.02	0.811	81.1	0.677 ± 0.028	0.907	90.7
	2×10^{-3}	0.036 ± 0.002	0.734	73.4	0.071 ± 0.004	0.816	81.6	0.328 ± 0.2	0.851	85.1	0.408 ± 0.024	0.942	94.2

yields a much higher inhibition efficiency at very low concentration. The demand for both better and more environmentally friendly surfactants has led to the formulation of these surfactants that have high performance and lower toxicity. This aspect adds to the practicality of using the present inhibitors under investigation. Furthermore, the cost effectiveness can be explained based on the fact that these inhibitors are used in really low concentrations.

To judge the durability of inhibitive performance of the tested inhibitor on a time scale, weight loss measurements were conducted in 1 M HCl solution in the presence of an optimum concentration of each inhibitor for 3−96 h immersion time at a temperature of 303 K. The variation of η_w (%) with various immersion times (t) is shown in Figure S4 (Supporting Information). η_w (%) increased from 71.04 to 93.39% for (C_{12}Cys) and 65.58 to 80.21% for 2(C_{12}Cys) when immersion time increased from 3 to 48 h. This displays the potent adsorption of inhibitor molecules on the MS surface, resulting in the formation of a more protective film at the MS/HCl solution interface. Thereafter, no significant change in η_w (%) was noted; 93.39−93.02% for (C_{12}Cys) and 80.21−79.2% for 2(C_{12}Cys). This is due to the negligible desorption of inhibitor molecules with increasing immersion time. It is evident that the studied inhibitors showed good inhibition of corrosion and stability over a long period of immersion of MS in acid solution.

2.5.2. Influence of Temperature and Activation Parameters. A comparison of the η_w of (C_{12}Cys) and 2(C_{12}Cys) for MS corrosion in HCl solution (Table 3) in the absence and presence of various concentrations of inhibitor at four temperatures (303, 313, 323, and 333 K) indicated that η_w enhanced with an increase in inhibitor concentrations, with an increase in temperature up to 333 K. The increase in η_w with a rise in temperature is indicative of chemisorption.[38] The temperature dependence of the corrosion rate can be expressed by the Arrhenius equation,[49] where the natural log of ν is a linear function with $1/T$, where ν is the corrosion rate, E_a is the energy of activation, R is the universal gas constant, and T is the absolute temperature.

$$\log(\nu) = \log A - E_a/2.303RT \quad (3)$$

On the basis of the gravimetric measurements, Figure S5a (Supporting Information) graphically represents the regression of log (ν) with an increase in $1/T$ for MS in the absence and presence of different concentrations of the synthesized (C_{12}Cys) and 2(C_{12}Cys) inhibitors, respectively. The straight lines indicate the linear relationship between log (ν) and $1/T$.

The E_a values at different temperatures were calculated from the slope, equal to $-E_a/R$ of each straight line, and are listed in Table 5. Generally, in the presence of both the synthesized inhibitors, the activation energy is lower than that in their absence, and a more obvious lowering in E_a is accompanied by a more efficient inhibitory effect with concentration of the synthesized inhibitors. The decrease in E_a with inhibitor concentration is typical of chemisorption. An alternative formulation of the Arrhenius equation[50] is shown below, where ν is the corrosion rate, N is the Avogadro number, h is the Planck's constant, R is the universal gas constant, T is the absolute temperature, ΔH^* is the enthalpy of the activation, and ΔS^* is the entropy of the activation.

$$\nu = \frac{RT}{Nh}\exp\left(\frac{\Delta S^*}{R}\right)\exp\left(-\frac{\Delta H^*}{RT}\right) \quad (4)$$

DOI: 10.1021/acsomega.7b00501
ACS Omega 2017, 2, 5691−5707

Table 4. Comparison of the Inhibition Efficiency of Studied Inhibitors with Other Surfactants Obtained for MS in Acidic Media Reported in the Literature

s. no	inhibitor	C_{inh} (M)	temp. (°C)	medium	η, %	ref
1.	(C_{12}Cys)	2×10^{-4}	30	1 M HCl	86	present study
2.	(*E*)-*N*-(3-((4-hydroxy-3-methoxybenzylidine)amino)propyl)-*N*,*N*-dimethylhexadecan-1-aminium	1×10^{-2}	25	1 M HCl	84	39
3.	nonionic surfactant based on amino acid (leucine)	5×10^{-5}	25	1 M HCl	83	40
4.	nonionic dithiol surfactants (PDP)	1×10^{-2}	25	1 M HCl	62	41
5.	1-dodecyl-methyl-1*H*-benzo[*d*][1,2,3]triazole-1-ium bromide (1-DMBT)	1×10^{-3}	25	1 M HCl	97	42
6.	alkyl dimethylisopropylammonium hydroxide cationic surfactants	1×10^{-2}	30	1 M HCl	93	43
7.	vanillin cationic surfactant	1×10^{-2}	25	1 M HCl	89	44
8.	2(C_{12}Cys)	2×10^{-6}	30	1 M HCl	84	present study
9.	2,2′-(pentane-1,5-diylidenebis(azan-1-yl-1-ylidene))bis(1- 1-dodecylpyridinium bromide) Gemini surfactant	1×10^{-2}	20	0.5 M H_2SO_4	97	45
10.	12-2-12	1×10^{-3}	25	1 M HCl	98	46
11.	18-triazole-18 GS	1×10^{-3}	25	1 M HCl	98	47
12.	SBGS-10	1×10^{-3}	50	1 M H_2SO_4	93	48

Table 5. Activation Parameters for MS Corrosion in 1 M HCl without and with Different Concentrations of (C_{12}Cys) and 2(C_{12}Cys) Inhibitors at 303−333 K

inhibitor	C_{inh} (M)	E_a	ΔH^*	ΔS^*
blank	0	113.03	110.42	0.159
(C_{12}Cys)	1×10^{-3}	102.32	99.70	0.115
	7×10^{-3}	100.45	97.82	0.106
	1×10^{-2}	93.47	91.19	0.083
	7×10^{-2}	92.85	90.24	0.079
	0.15	83.07	80.45	0.045
	0.2	85.01	82.38	0.050
2(C_{12}Cys)	5×10^{-5}	106.52	103.90	0.133
	1×10^{-4}	103.62	101.00	0.121
	5×10^{-4}	99.89	97.27	0.108
	8×10^{-4}	89.52	86.90	0.072
	1.2×10^{-3}	85.65	83.03	0.058
	2×10^{-3}	73.00	70.39	0.017

Plotting $\log(\nu/T)$ against $1/T$ yields straight lines, as shown in Figure S5b (Supporting Information). Values of ΔH^* and ΔS^* were calculated from the slope $-(\Delta H^*/2.303R)$ and intercept $\log(R/Nh) + (\Delta S^*/2.303R)$, respectively (Table 5). Assessment of Table 5 shows that the values of E_a, ΔH^*, and ΔS^* varied in an identical manner. The positive sign of the enthalpy (ΔH^*) reflected the endothermic nature of the MS dissolution process. ΔS^* in the presence of surfactants (C_{12}Cys) or 2(C_{12}Cys) was less than that in the blank; this implies that disorder on the MS surface decreased.[51]

2.5.3. Adsorption Isotherm and Thermodynamic Calculations. From gravimetric data, it is possible to determine the values of the degree of MS surface coverage, θ, as a function of (C_{12}Cys) or 2(C_{12}Cys) concentration. The calculated values of θ were fitted to several kinds of adsorption isotherms (e.g., Temkin, Frumkin, and Langmuir isotherms), but excellent fitting was observed for the Langmuir adsorption isotherm model. In this model, θ is related to the concentration of the inhibitor (C_{inh}) by the following equation.

$$C_{inh}/\theta = 1/K_{ads} + C_{inh} \quad (5)$$

where K_{ads} stands for the equilibrium constant in the adsorption process. A linear relationship between C_{inh}/θ versus C_{inh} was observed with a strong correlation coefficient (R^2). In Figure 4, the values of R^2 for the Langmuir adsorption model are close to 1

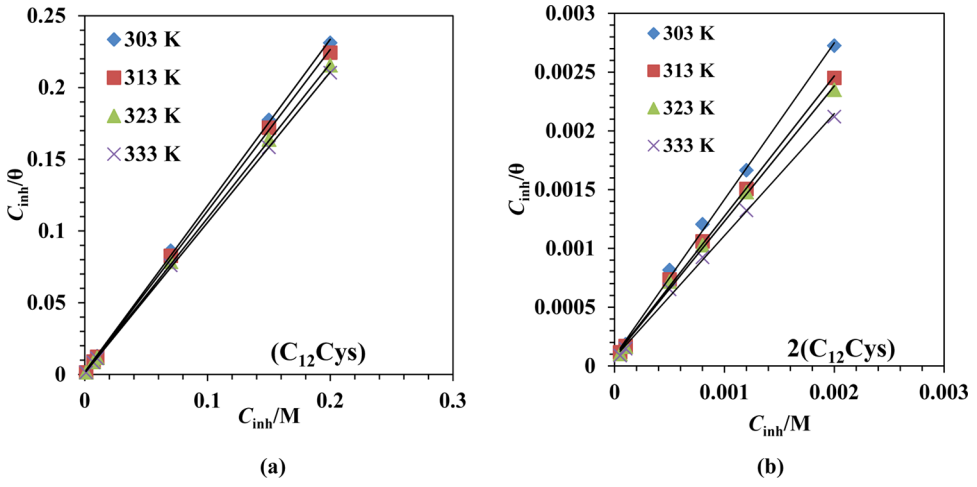

Figure 4. Langmuir adsorption isotherm plots for MS in 1 M HCl solution containing various concentrations of (a) (C_{12}Cys) and (b) 2(C_{12}Cys) at 303−333 K.

DOI: 10.1021/acsomega.7b00501
ACS Omega 2017, 2, 5691−5707

Table 6. Thermodynamic Parameters of Adsorption for MS in 1 M HCl at Different Temperatures

inhibitor	temp. (K)	K_{ads}	ΔG°_{ads} (kJ mol^{-1})	ΔH°_{ads} (kJ mol^{-1})	ΔS°_{ads} (J mol^{-1} K^{-1})	ΔH°_{ads}[a] (kJ mol^{-1})	ΔS°_{ads}[a] (J mol^{-1} K^{-1})
(C_{12}Cys)	303	555.55	−26.18	13.39	−0.130	13.59	−0.130
	313	625	−27.55		−0.086		
	323	714.28	−28.85		−0.088		
	333	909.09	−29.98		−0.090		
2(C_{12}Cys)	303	11 363.64	−33.64	6.10	−0.131	6.22	−0.131
	313	11 904.76	−34.87		−0.111		
	323	12 500.21	−36.12		−0.112		
	333	14 285.71	−37.60		−0.113		

[a]Values are obtained from the verification plot of ΔG°_{ads} vs T.

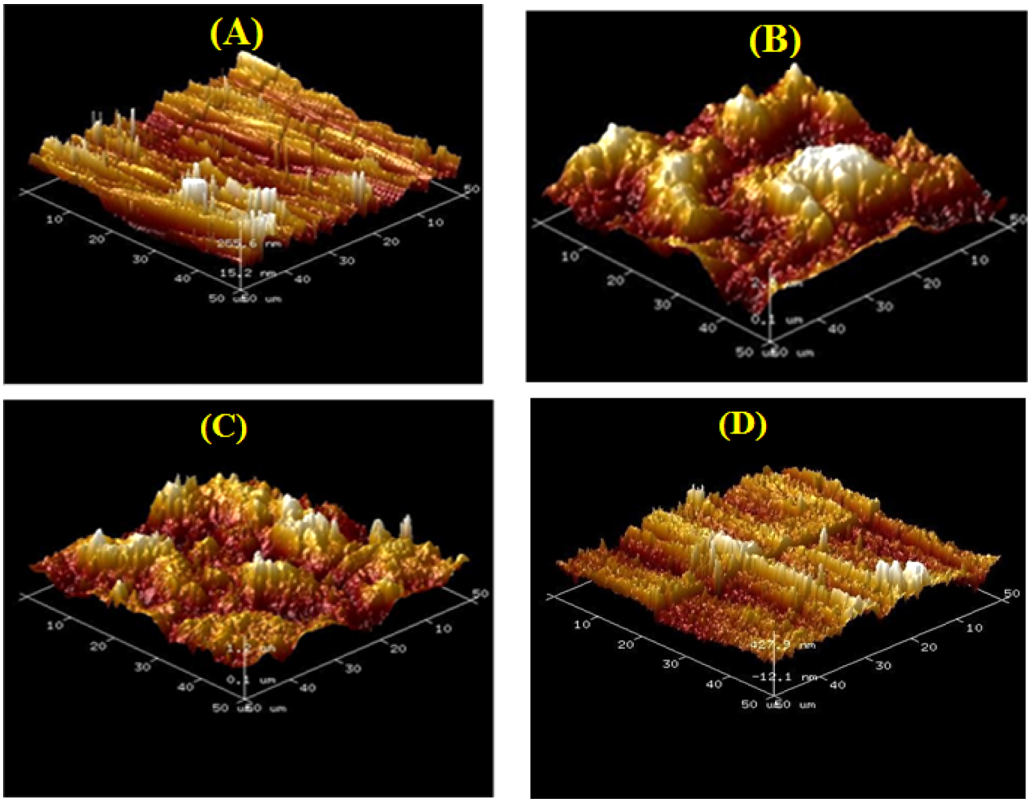

Figure 5. AFM images of MS after 6 h immersion in 1 M HCl solution: (A) polished MS prior to immersion, (B) uninhibited solution, and (C) acid solution with 0.2 mM (C_{12}Cys) and (D) 0.002 mM 2(C_{12}Cys).

for both inhibitors. Higher values of K_{ads} (Table 6) suggest stronger adsorption of the inhibitor molecules on the metal surface and hence better inhibition efficiency.[52]

With increasing temperature, the values of K_{ads} increased, implying that 2(C_{12}Cys) and (C_{12}Cys) are easily and strongly adsorbed onto the MS surface at relatively higher temperatures.

The standard free energy of adsorption, ΔG°_{ads}, is related to K_{ads} by the following equation.

$$K_{ads} = \left(\frac{1}{55.5}\right) \exp\left(\frac{-\Delta G^{\circ}_{ads}}{RT}\right) \quad (6)$$

where 55.5 is the molar concentration of water in the solution expressed in M, R is the gas constant (8.314 J K^{-1} mol^{-1}), and T is the absolute temperature (K). The negative values of ΔG°_{ads} (Table 6) confirm the spontaneity of the adsorption process and stability of the adsorbed surfactant layer on the MS surface. ΔG°_{ads} values range between −26.18 and −37.60 kJ mol^{-1} for both the studied inhibitors (Table 6); this specifies that the adsorption of (C_{12}Cys) and 2(C_{12}Cys) molecules on the MS surface involves physisorption along with chemisorption.[53]

As thermodynamic models are useful for describing the mechanism of an inhibitor's adsorption on a metal surface, the heat of adsorption, ΔH°_{ads}, was deduced using the van't Hoff equation.

$$\log K_{ads} = -\left(\frac{\Delta H^{\circ}_{ads}}{RT}\right) + \text{constant} \quad (7)$$

The plot of log K_{ads} versus $1/T$ for (C_{12}Cys) is given in Figure S6a (Supporting Information), and the figure for 2(C_{12}Cys) is not shown here. The absorptive heat (ΔH°_{ads}) was approximated from the slope of this graph and is presented in Table 6. The positive value of ΔH°_{ads}, 12.23 kJ mol^{-1} for (C_{12}Cys) and 6.10 kJ mol^{-1} for 2(C_{12}Cys), discloses that the adsorption of 2(C_{12}Cys) or (C_{12}Cys) molecules on MS is an endothermic process, which is generally attributed to chemisorption.[54] Again, another thermodynamic parameter (ΔS°_{ads}) was obtained using the equation

DOI: 10.1021/acsomega.7b00501
ACS Omega 2017, 2, 5691−5707

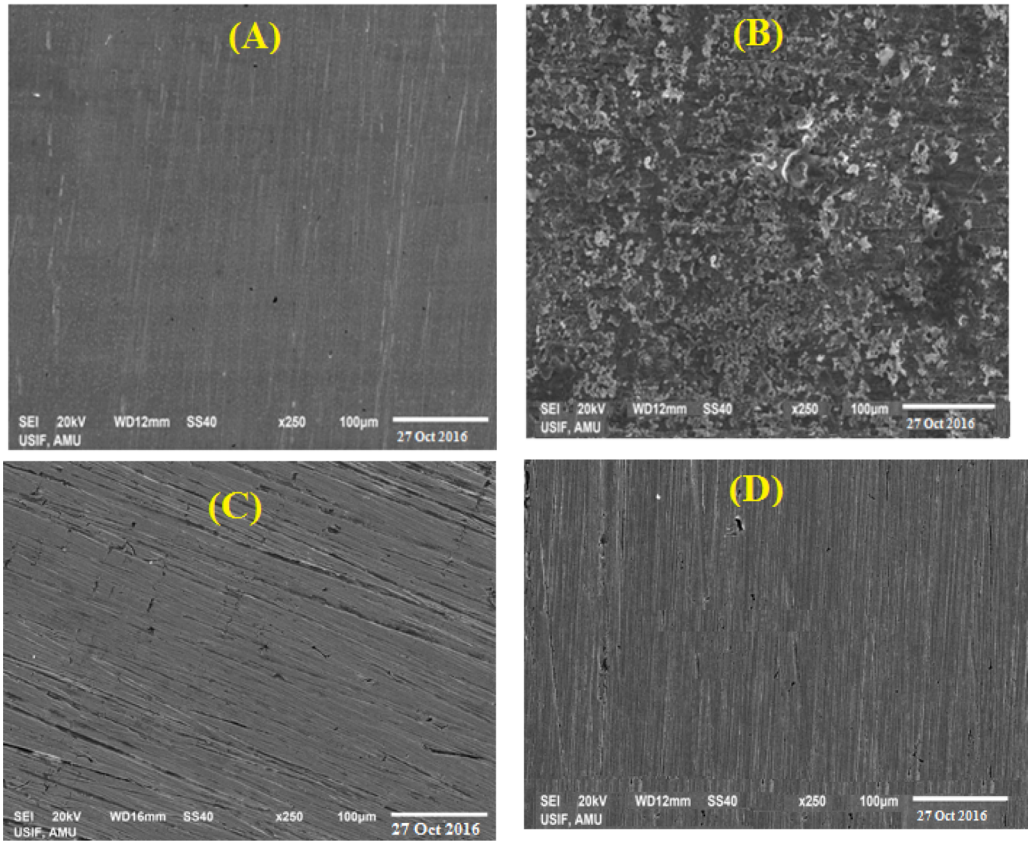

Figure 6. SEM images of MS after 6 h immersion in 1 M HCl solution: (A) polished MS prior to immersion, (B) uninhibited solution, and (C) acid solution with 0.2 mM (C_{12}Cys) and (D) 0.002 mM 2(C_{12}Cys).

$$\Delta G^{\circ}_{ads} = \Delta H^{\circ}_{ads} + T\Delta S^{\circ}_{ads} \quad (8)$$

The values of ΔS°_{ads} for (C_{12}Cys) and 2(C_{12}Cys) are negative, which might be due to the orderly adsorption of their molecules on the MS substrate causing a considerable decrease in the values of entropy.

The variation of ΔG°_{ads} with $1/T$ yields a straight line with a slope that equals ΔH°_{ads} = 12.20 kJ mol^{-1} (Figure S6b). The ΔH°_{ads} values found by the two methods are in good agreement.

2.6. Surface Characterization. Figure 5A–D depicts the AFM images of the surface topographies for MS prior to immersion and after immersion in 1 M HCl solution without and with the studied inhibitors. A very rough surface topography for the uninhibited system and a pronounced reduction in surface roughness for the inhibited system is evident. The corresponding average surface roughness (R_a) (calculated with the associated software) of the polished MS surface prior to immersion was observed to be 70.8 nm (Figure 5A). In the absence of (C_{12}Cys) or 2(C_{12}Cys), the surface displayed an extremely rough topography (Figure 5B) due to an unhindered corrosion attack and the R_a increased from 70.8 to 627 nm. In the presence of (C_{12}Cys) and 2(C_{12}Cys), the MS shows a smoother surface and the R_a value decreased from 627 to 290 nm for (C_{12}Cys) (Figure 5C) and 118.6 nm for 2(C_{12}Cys) (Figure 5D).

The SEM micrographs of the polished MS specimen and those of MS exposed to the uninhibited and inhibited acid solutions are shown in Figure 6A–D. A close look at the SEM images obtained after MS immersion in 1 M HCl solution without (Figure 6B) and with 0.2 mM C_{12}Cys (Figure 6C) or 0.002 mM 2C_{12}Cys (Figure 6D) revealed a rougher surface for the uninhibited system compared with that of the inhibited system. This is attributed to the shielding imparted by the adsorption of inhibitor molecules onto the MS surface. The better inhibitive potential of 2(C_{12}Cys) compared to that of (C_{12}Cys) is also reflected as the surface of the MS in Figure 6D shows a closer resemblance to the freshly polished MS surface.

Figure 7 presents the EDAX spectra recorded for MS samples exposed for 6 h in 1 M HCl solution in the absence and presence of optimum concentrations of (C_{12}Cys) and 2(C_{12}Cys).

The EDAX spectrum of the polished surface (Figure 7A) shows the characteristic peaks of the elements comprising the MS. The EDAX analysis of the MS surface in HCl solution (Figure 7B) revealed that the surface film contains mainly Fe with small percentages of C, O, and Cl. Further, Fe peaks are considerably suppressed and Fe content is appreciably reduced from 95% (for polished MS) to 67.56% (for MS in HCl solution). This shows that Fe corrosion takes place through the formation of iron oxides or iron chlorides. In the presence of (C_{12}Cys) and 2(C_{12}Cys) (Figure 7C,D), the EDAX spectra show additional peaks of N and S, and an enhancement in the intensity of Fe peaks to 78.3 and 82.3%, respectively.

These data show that inhibitors having N along with S atoms have covered the electrode surface resulting in a lowering of the extent of acid corrosion. However, the signals appreciably strengthen upon adding 2(C_{12}Cys) to the HCl solutions. This is undoubtedly due to the high contribution of the N and S in the presence of 2(C_{12}Cys). This shows that more 2(C_{12}Cys) is adsorbed on the MS surface, thus confirming the results obtained from the weight loss and electrochemical measurements.

2.7. Quantum Chemical Calculation. Before carrying out the theoretical calculations, ACD/Labs commercial software was

DOI: 10.1021/acsomega.7b00501
ACS Omega 2017, 2, 5691–5707

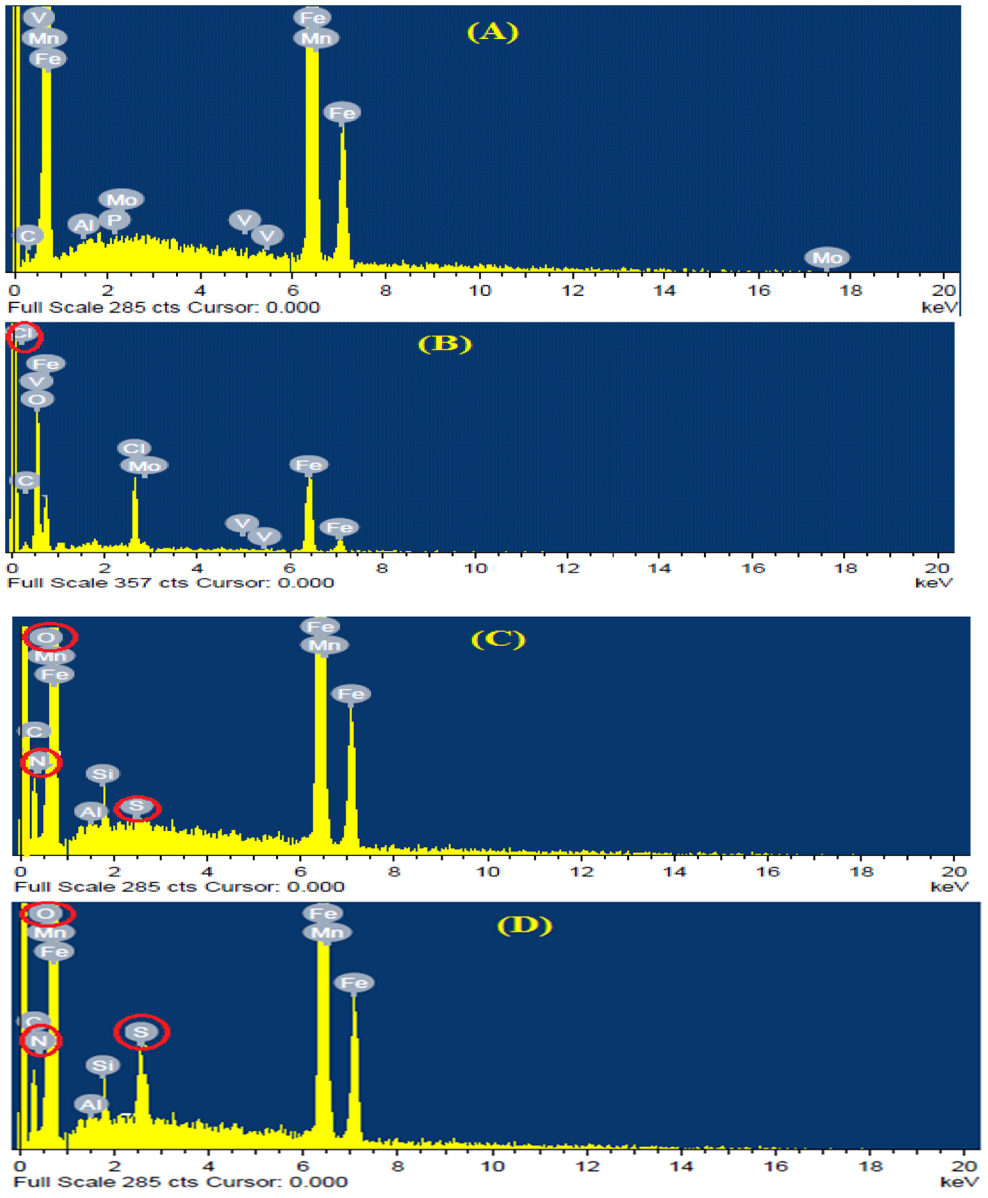

Figure 7. EDAX images of MS after 6 h immersion in 1 M HCl solution: (A) polished MS prior to immersion, (B) uninhibited solution, and (C) acid solution with 0.2 mM (C_{12}Cys) and (D) 0.002 mM 2(C_{12}Cys).

utilized to determine the major species of (C_{12}Cys) and 2(C_{12}Cys) in 1 M HCl.

The calculations of the (−NH) pK_a values of the two inhibitors (2.0 for (C_{12}Cys) and 1.4 for 2(C_{12}Cys)) indicate that they are easily protonated and form cationic forms in acid media. Therefore, their protonated forms, as depicted in Figure 8, were used for quantum chemical calculations as well as Monte Carlo simulation to simulate their realistic molecular structures in acid medium.

Figure 9 shows the results of the optimized structures, and highest occupied molecular orbital (HOMO) and lowest unoccupied molecular orbital (LUMO) distributions for protonated (C_{12}Cys) and 2(C_{12}Cys). As can be seen in Figure 9, the HOMO densities for the two molecules are located on the long carbon chain. For the LUMO electron densities, there was a clear difference.

Although the LUMO of (C_{12}Cys) was found on the −SH, −NH, and COOH groups, the LUMO of 2(C_{12}Cys) was concentrated on the two −NH and the disulfide −S−S− groups. The presence of the HOMO orbitals on the long carbon chains could make it easier for the two molecules to adsorb in a parallel manner onto a steel surface, as shall be seen from the Monte Carlo simulation results. HOMO and LUMO, the frontier molecular orbitals, are widely used to anticipate the adsorption centers of inhibitor molecules.[55] E_{HOMO} indicates the propensity of a molecule to donate electrons. The higher the E_{HOMO}, the greater the ability of that molecule to donate electrons. E_{LUMO} indicates the propensity of a molecule to accept electrons. The lower the E_{LUMO}, the greater the ability of that molecule to accept electrons. Energy gap, hardness, and softness are reactivity indices that can be used to probe the ease of reactivity and stability of a Lewis base (inhibitor) and a Lewis acid (metal) using the hard and soft acid and base theory (HSAB).

The HSAB description is important in understanding the predominant factors that drive chemical properties and reactions of corrosion inhibitors with metal surfaces. The energy gap, ΔE, indicates the reactivity propensity of a molecule toward the metal surface. As ΔE decreases, the reactivity of the molecule increases,

DOI: 10.1021/acsomega.7b00501
ACS Omega 2017, 2, 5691−5707

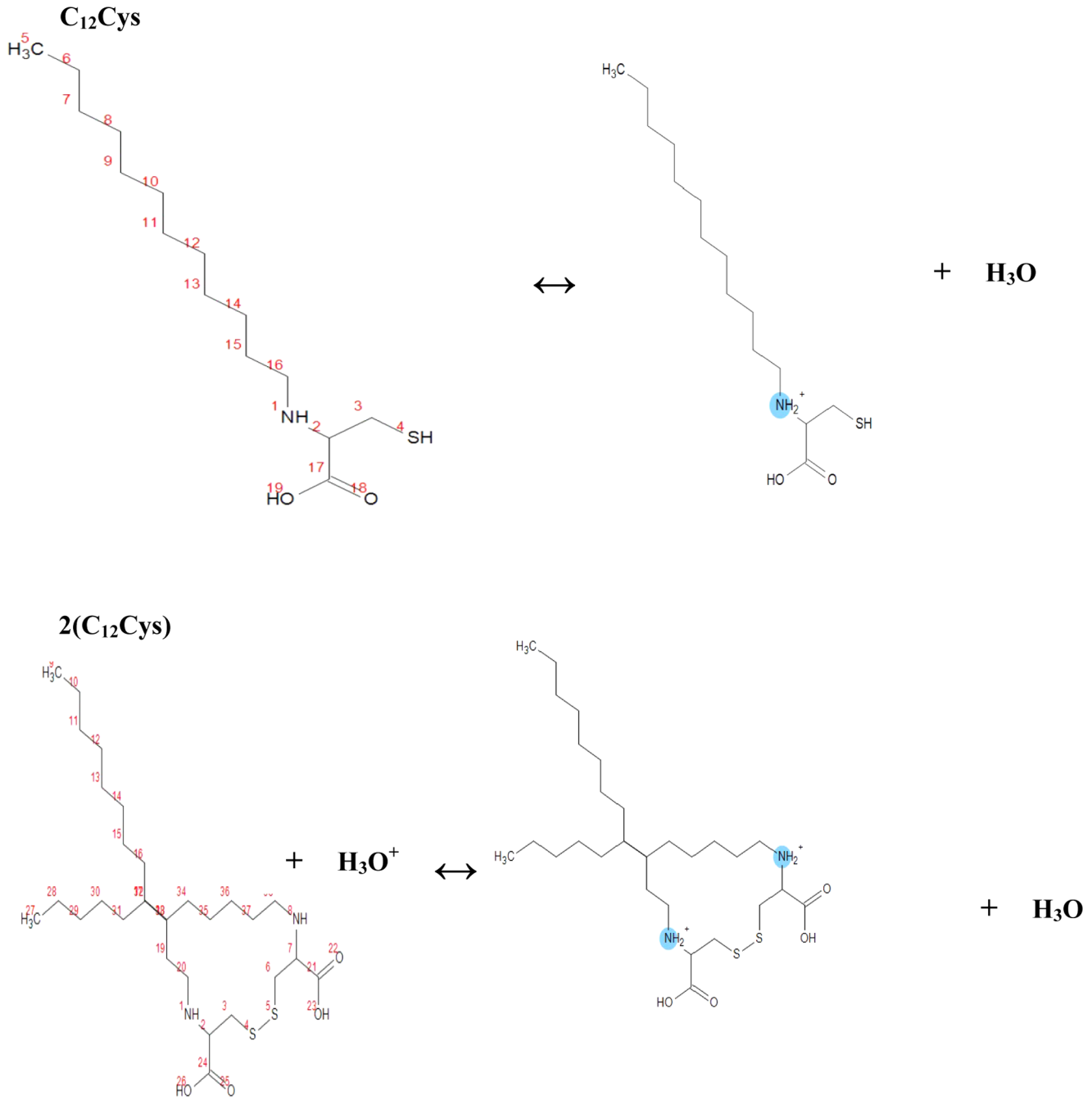

Figure 8. Protonation process of (C_{12}Cys) and 2(C_{12}Cys) in acidic medium.

leading to an enhancement in the adsorption onto a metal surface.[56]

According to the quantum chemical results obtained from Table 7, (C_{12}Cys) has more electron donating ability than 2(C_{12}Cys). On the other hand, 2(C_{12}Cys) has a higher propensity to accept electrons from the d-orbital of Fe than (C_{12}Cys). This higher capacity of accepting electrons (retro-donation) from Fe can strengthen the interaction between 2(C_{12}Cys) and steel when compared with (C_{12}Cys). The energy gap, ΔE, decreases as follows: 2(C_{12}Cys) < (C_{12}Cys). It is clear from the above ranking that if the ordering of ΔE is considered, 2(C_{12}Cys) is expected to be a more reactive and effective corrosion inhibitor than (C_{12}Cys). This theoretical finding is in good agreement with the experimental results. According to Koopmen's theorem, the values of E_{HOMO} and E_{LUMO} of the inhibitor molecule are associated with the ionization potential (I) and the electron affinity (A), respectively. The values of I and A are defined as $-E_{HOMO}$ and $-E_{LUMO}$, respectively,[57] and the obtained values were used to calculate the global hardness (η) and the electronegativity[58] (χ).

$$\eta = \frac{I - A}{2} \tag{9}$$

$$\chi = \frac{I + A}{2} \tag{10}$$

$$\sigma = \frac{1}{\eta} = \frac{2}{I + A} \tag{11}$$

DOI: 10.1021/acsomega.7b00501
ACS Omega 2017, 2, 5691−5707

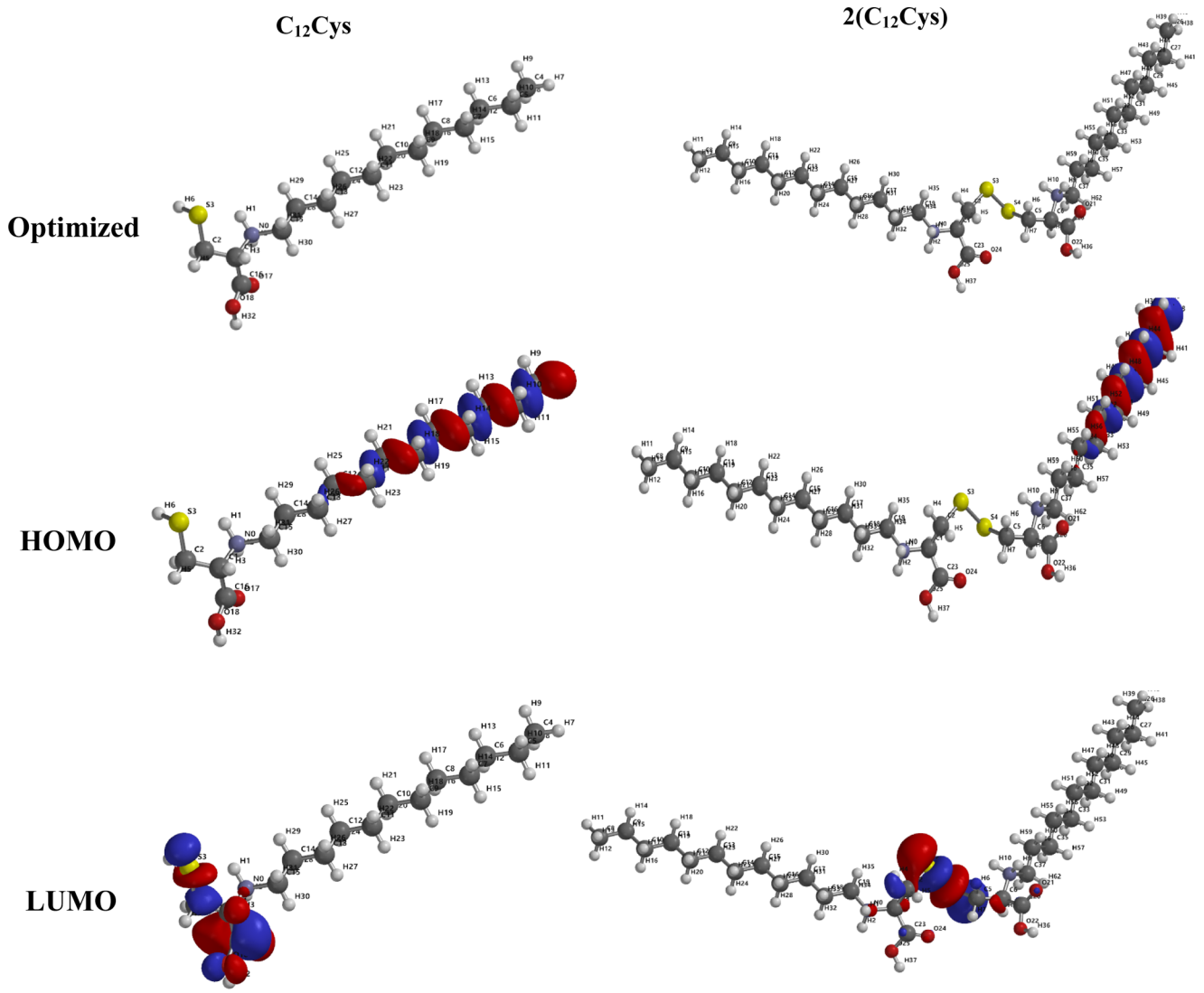

Figure 9. Optimized structures, and HOMO and LUMO energies of (C_{12}Cys) and 2(C_{12}Cys).

Table 7. Quantum Chemical Parameters for Protonated Forms of (C_{12}Cys) and 2(C_{12}Cys) Calculated Using Density Functional Theory at B3LYP/6-31G (d,p) Level of Theory

inhibitor	E_{HOMO} (eV)	E_{LUMO} (eV)	ΔE (eV)[a]	I	A	η	σ	χ	ΔN
(C_{12}Cys)	−9.48	−4.71	4.77	9.48	4.71	2.38	0.419	2.381	0.967
2(C_{12}Cys)	−10.27	−7.14	3.13	10.27	7.14	1.56	0.638	1.565	1.736

[a] $\Delta E = E_{LUMO} - E_{HOMO}$.

The calculated values of χ are also mentioned in Table 7, and show the tendency of an atom to attract the shared pair of an electron toward itself.[13] Absolute hardness, η, determines both the stability and reactivity of a molecule, which suggests the resistivity of an inhibitor for the physical adsorption process. Soft molecules with small energy gaps are far more reactive than hard ones with large energy gaps, as they could readily offer electrons to an acceptor.

The fraction of electrons transferred (ΔN) from the inhibitor to the MS surface can be calculated by eq 17[49] using the χ and η values.

$$\Delta N = \frac{\chi_{Fe} + \chi_{inh}}{2(\eta_{Fe} + \eta_{inh})} \quad (12)$$

where χ_{Fe} and χ_{inh} represent the electronegativity and η_{Fe} and η_{inh} represent the absolute hardness of iron and the inhibitor molecules, respectively. The theoretically calculated value of χ_{Fe} for iron metal is 7 eV mol^{-1} and η_{Fe} is 0 eV mol^{-1}. These values were appropriately substituted to calculate ΔN.

The values of ΔN exhibit the path of the electron transfer between inhibitor and metal surface. ΔN exhibits the inhibitive performance of the inhibitors resulting from electron donation. In the current investigation, ΔN values are >0 and <3.6, indicating electron transfer from the inhibitors to the MS surface.[59−61]

2.8. Monte Carlo Simulations. The interaction between the two corrosion inhibitors investigated, namely, protonated (C_{12}Cys) and 2(C_{12}Cys), with the Fe (110) surface was carried out to locate the low energy adsorption configuration and the

DOI: 10.1021/acsomega.7b00501
ACS Omega 2017, 2, 5691−5707

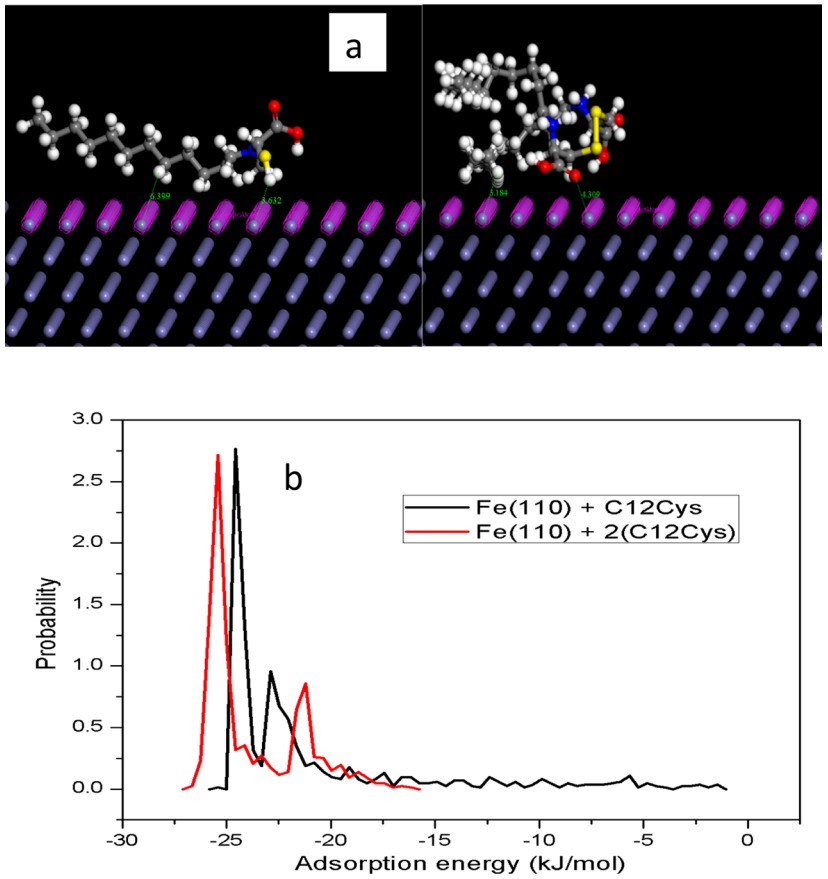

Figure 10. (a) Model Structures simulating the adsorption of (C_{12}Cys) and 2(C_{12}Cys) on the Fe surface. (b) Probability distribution curves in adsorption energy function for (C_{12}Cys) and 2(C_{12}Cys) on the Fe surface.

electron transfer process that takes place at the steel/electrolyte interface. Figure 10a shows the equilibrium adsorption configurations of (C_{12}Cys) and 2(C_{12}Cys) with a stable Fe(110) crystallographic plane.

As can be seen in Figure 10a, (C_{12}Cys) is adsorbed in a parallel orientation to the metal surface whereas 2(C_{12}Cys) has a twisted geometry due to the deformation of the molecule. Furthermore, the N, S, and O heteroatoms of 2(C_{12}Cys) adsorbed closer to the metal surface when compared to the heteroatoms present in (C_{12}Cys). This indicates a stronger interaction of 2(C_{12}Cys) than (C_{12}Cys). Figure 10b shows the probability distribution curves for the adsorption energies of the two inhibitors on the Fe(110) surface. It can be seen that 2(C_{12}Cys) has a higher negative adsorption energy than (C_{12}Cys), which suggests a stronger interaction of the inhibitor molecules with the metal surface.[56,62] We conclude from the results obtained that the interaction between 2(C_{12}Cys) and the steel surface is greater than that of (C_{12}Cys). This result indicates that 2(C_{12}Cys) is expected to inhibit steel corrosion in 1 M HCl solution more than (C_{12}Cys). The theoretical results are in good agreement with the experimental results.

2.9. Mechanism of Corrosion Inhibition. In general, the inhibition effect of the amino acid based monomeric and Gemini surfactants is due to the adsorption of their molecules on the metal surface via $-NH_2$, $-COOH$, and $-SH$ groups. The MS surface in HCl solution is positively charged,[15,62] which favors the adsorption of negatively charged Cl^- ions from the HCl solution at the MS/electrolyte interface thus changing the charge on the solution side of the interface to negative from positive. As reported in Section 2.7 (quantum chemical calculations), in 1 M HCl solution, the studied inhibitors easily get protonated and remain predominantly in the cationic form. The negatively charged metal surface (due to adsorption of Cl^- ions) is suitable for the adsorption of cations in acidic solution.[63] Thus, the chloride ions promote the physical adsorption of the studied inhibitor molecules on the MS surface. Additionally, the inhibitor molecules may be chemically adsorbed on the MS surface due to formation of coordinate type bonds between the vacant orbital of Fe atoms and the lone pairs of electrons of the unprotonated S and N atoms. In addition, there may be direct adsorption of the cationic species on the cathodic sites of the MS, which may hinder the hydrogen evolution reaction whereas the lone pair of electrons on S atoms may promote adsorption on the anodic sites.[64]

3. CONCLUSIONS

1. The amino acid based monomeric and Gemini surfactants referred to as (C_{12}Cys) and 2(C_{12}Cys) were synthesized and characterized. These compounds exhibited surface active properties and acted as good inhibitors in preventing corrosion of MS steel in 1 M HCl solution.
2. A potentiodynamic polarization study showed that (C_{12}Cys) and 2(C_{12}Cys) act as mixed-type inhibitors in acidic solution, diminishing both anodic and cathodic corrosion.
3. The weight loss measurement results showed that (C_{12}Cys) and 2(C_{12}Cys) are effective inhibitors for MS corrosion in 1 M HCl solutions.

DOI: 10.1021/acsomega.7b00501
ACS Omega 2017, 2, 5691−5707

4. An increase in (C_{12}Cys) or 2(C_{12}Cys) concentration and electrolyte temperature resulted in an increase in inhibition efficiency. However, in comparison to (C_{12}Cys), 2(C_{12}Cys) showed high corrosion inhibition efficiency at comparatively low concentration.
5. High inhibition efficiencies exhibited by the inhibitors were attributed to their adherent adsorption and the adsorption fitted Langmuir's kinetic/thermodynamic model.
6. The results obtained from weight loss, polarization, and EIS techniques are in good agreement.
7. AFM and SEM/EDAX images are suggestive of a smoother MS surface in (C_{12}Cys) or 2(C_{12}Cys) inhibited acid solution compared to that in the uninhibited system.
8. Experimental findings were adequately supported by quantum chemical calculations and Monte Carlo simulations.

4. EXPERIMENTAL SECTION

4.1. Chemicals. Cysteine (97%), cystine (98%), and *n*-doceylbromide (98%) were procured from Sigma-Aldrich. Acetone (99%), methanol (99%), (s.d.fine-chem limited), hexane (Merck), thymopthalein (kemphasol), NaOH (97%) (emplura), and 37% HCl (99.5%) (Fisher Scientific, India) were used as received.

4.2. Specimen Composition and Solution. Rectangular specimens of dimension 2.5 cm × 2 cm × 0.1 cm (exposed surface area 10.9 cm^2) were cut from a MS sheet, obtained commercially, and utilized for weight loss measurements. For electrochemical measurements, circular specimens (exposed surface area 1.0 cm^2) were used. The chemical composition (wt %) of MS, as obtained by spark optical emission spectrometry, is as follows: C-0.06109, Cr-0.03506, Mn-0.18145, Mo-0.05399, P-0.01775, Al-0.01736, V-0.03357, and Fe-99.59. Prior to a weight loss or electrochemical experiment, the MS surface was successively abraded with mechanical grade emery papers of 320−1200 grade. Before using the specimen in weight loss measurements or as a working electrode (WE) in electrochemical measurements, it was well cleaned, degreased with ethanol, washed with double-distilled water, and finally dried in warm air.

Blank (1 M HCl) solution was prepared by diluting analytical grade HCl (37%) with double-distilled water. For corrosion measurements, the concentration range of surfactants varied from 1×10^{-3} to 0.2 mM for (C_{12}Cys) and 5×10^{-5} to 0.002 mM for 2(C_{12}Cys). The test solutions in all measurements were made using double-distilled water.

4.3. Chemical Synthesis of Inhibitors. (C_{12}Cys) and 2(C_{12}Cys) used in this work were synthesized and purified as reported[25] and the detailed procedure is given in the Supporting Information (Scheme S1).

4.4. Surface Tension Measurement. Surface tension (γ) of 2(C_{12}Cys) and (C_{12}Cys) solutions in 1 M HCl was determined as a function of their concentration on a Kruss tensiometer K11 MK3 (Germany) using the ring tear-off method. To equilibrate, the solutions of surfactants were placed at room temperature for 15 min. Values of γ decrease continuously and then become constant along a wide concentration range. When the constancy of γ begins, the point of break was considered as the CMC of the system.

4.5. Electrochemical Measurements. The electrochemical measurements were done in an AUTOLAB 1L corrosion cell (three neck) with a Ag/AgCl electrode, provided with a luggin capillary probe as reference electrode along with Pt foil as counter electrode. A MS coupon, which acted as the working electrode (WE) was attached to a specially designed holder. To minimize IR drop, the tip of the luggin probe was placed very close to the surface of the WE. The measurements were accomplished by an Autolab potentiostat/galvanostat, model 128 N, with an inbuilt impedance analyzer FRA 2 at 303 K under unstirred conditions. Prior to the commencement of an experiment, the potential was continuously monitored until it stabilized and a steady-state open-circuit potential (OCP) was achieved.

For the anodic and cathodic polarization curves, an overpotential voltage of −250 mV versus Ag/AgCl to +250 mV versus Ag/AgCl with reference to OCP was applied at a scan rate of 0.1 mV s^{-1}. Corrosion current density (I_{corr}), equilibrium corrosion potential (E_{corr}), anodic Tafel slope (β_a), and cathodic Tafel slope (β_c) values were obtained using NOVA 1.11 software. Inhibition efficiency (η_{PDP}) and surface coverage (θ) at different inhibitor concentrations were calculated by the equations given below, where I_{corr} and $I^{(i)}_{corr}$ are the corrosion current densities without and with inhibitor, respectively.

$$\eta_{PDP}\ (\%) = \theta \times 100 \tag{13}$$

$$\theta = \frac{I_{corr} - I^{(i)}_{corr}}{I_{corr}} \tag{14}$$

Impedance spectra were obtained at OCP within the frequency domain of 10^{-2}−10^5 Hz by applying 10 mV sine wave AC voltage. Before starting experiments, the electrochemical system was stabilized to gather EIS data at OCP. The obtained EIS spectra were analyzed for the values of R_{ct}, charge transfer resistance, and C_{dl}, double layer capacitance. Inhibition efficiency (η_{EIS}) was computed at each inhibitor concentration with the help of the following equation.

$$\eta_R(\%) = \frac{R_{ct}^{(i)} - R_{ct}}{R_{ct}^{(i)}} \tag{15}$$

where R_{ct} and $R_{ct}^{(i)}$ are the charge transfer resistances without and with surfactant, respectively.

4.6. Gravimetric Measurement. The gravimetric measurements were done in a 250 mL glass beaker positioned in a water bath with thermostat control. The MS specimens were weighed and suspended in 100 mL of electrolyte with and without (C_{12}Cys) or 2(C_{12}Cys) for 6 h at 303, 313, 323, and 333 K. As the tests were completed, the coupons were picked out, rinsed with double-distilled water, the corrosion product stripped off the sample surface with a soft nylon brush, thoroughly dried, and weighed. Measurements were done in triplicate to ensure high accuracy and the mean values of the corrosion rates were reported.

The corrosion rate (ν) and η_w (%) at various concentrations of 2(C_{12}Cys) or (C_{12}Cys) were obtained by following the below equation where w_1 and w_2 are the weight loss before and after immersion, respectively, A represents the surface area of the coupon (cm^2), and T is the exposure time (h).

$$\nu = \frac{w_1 - w_2}{AT} \tag{16}$$

$$\eta_w = \frac{\nu_o - \nu_i}{\nu_o} \times 100 \tag{17}$$

DOI: 10.1021/acsomega.7b00501
ACS Omega 2017, 2, 5691−5707

4.7. Surface Characterization: SEM/EDAX and AFM. Surface characterization studies were accomplished to find out the extent of corrosion damage in the absence and presence of the inhibitors in terms of surface roughness/heterogeneity, which in turn gave an idea about the extent of protection offered by the adsorbed surfactant layer. For SEM/EDAX and AFM analysis, the MS coupons of size 2.5 × 2.0 × 0.1 cm^3 were prepared as described above, this was followed by their immersion in the test solution without and with optimum concentrations of inhibitor for 6 h. After completion of immersion, the specimens were retrieved, the corrosion products removed mechanically, and the specimens were thoroughly rinsed with distilled water, dried, and subjected to AFM and SEM/EDAX analysis. The AFM analysis was done at room temperature in tapping mode in air using an AFM-Dimension icon ScanAsyst equipped with a Nanoscope V. The scan rate and scanning area were 0.4 Hz and 50 × 50 μm^2, respectively. The SEM images were obtained with a scanning electron microscope (model: JEOL JSM- 6510LV) with EDAX attachment (model: INCA, Oxford).

4.8. Quantum Chemical and Monte Carlo Simulations. Quantum chemical calculation was done using the density functional theory implemented in the Spartan'14 v1.1.8 software. The exchange−correlation was treated using a hybrid, B3LYP functional. A full optimization was performed using the 6-31G (d,p) basis sets. Molecular properties relevant to the activity of the molecules as corrosion inhibitors such as energy of the highest occupied orbitals (E_{HOMO}), energy of the unoccupied molecular orbitals (E_{LUMO}), energy gap (ΔE), electron affinity (E), ionization potential (I), hardness (η), softness (σ), and electronegativity (χ) were obtained.

The interaction between 2(C_{12}Cys) or (C_{12}Cys) and the MS surface was undertaken using Monte Carlo simulations. Adsorption Locator module in the Material Studio Software 7.0 (BIOVIA-Accelrys) was employed for the simulations. The simulation was done with Fe(110) crystal with a slab of 5 Å in depth with periodic boundary conditions. This ensured the simulation was of a representative part of an interface devoid of any arbitrary boundary effects. An Fe(110) plane was enlarged to a (12 × 12) super cell to provide a large surface for the interaction of 2(C_{12}Cys)/(C_{12}Cys). Thereafter, a vacuum slab with 50 Å thickness was built above the Fe(110) plane. The Fe(110) surface was fixed before simulations. To optimize the structures of all components of the system of interest during the whole simulation procedure, a universal force field was used.

■ ASSOCIATED CONTENT

Supporting Information

The Supporting Information is available free of charge on the ACS Publications website at DOI: 10.1021/acsomega.7b00501.

Variation in surface tension versus concentration for (C_{12}Cys) and 2(C_{12}Cys); variation of E_{OCP}−time curves for MS in uninhibited and inhibited 1 M HCl solution (temperature 303 ± 2 K); Randles equivalent circuit used to fit the impedance data; variation of η_w with immersion time (t); Arrhenius plots for MS in 1 M HCl in the absence and presence of different concentrations of (C_{12}Cys) and 2(C_{12}Cys), alternative Arrhenius plots for MS in 1 M HCl in the absence and presence of different concentrations of (C_{12}Cys) and 2(C_{12}Cys); linear regression between log K_{ads} and 1/T, verification plot of ΔG°_{ads} versus T; surface active parameters of (C_{12}Cys) and 2(C_{12}Cys) in 1 M HCl solution; detailed chemical synthesis and characterization of inhibitors (PDF)

■ AUTHOR INFORMATION

Corresponding Author

*E-mail: drmmobin@hotmail.com. Tel.: + 91-9411491161. Fax: + 91-571-2701895.

ORCID

Mohammad Mobin: 0000-0003-4829-7491

Ime B. Obot: 0000-0002-2700-9529

Eno E. Ebenso: 0000-0002-0411-9258

Notes

The authors declare no competing financial interest.

■ ACKNOWLEDGMENTS

One of the authors, Ruby Aslam, gratefully acknowledges financial support by UGC in the form of a MAN (Maulana Azad National) fellowship (2013-14-MANF-MUS-UTT-21927). The authors feel privileged to acknowledge Aligarh Muslim University USIF (University Sophisticated Instruments Facility) for SEM/EDAX and are also thankful to Central Drug Research Institute (CDRI), Lucknow, for providing the ^{1}H NMR facility. I. B. Obot is grateful to King Fahd University of Petroleum and Minerals, (KFUPM) Saudi Arabia, and the Centre of High Performance Computing (KFUPM) for making the computational software available for this work.

■ REFERENCES

(1) Kumar, S.; Vashisht, H.; Olasunkanmi, L. O.; Bahadur, I.; Verma, H.; Goyal, M.; Singh, G.; Ebenso, E. E. Polyurethane based tri-block-copolymers as corrosion inhibitors for mild steel in 0.5 M H2SO4. *Ind. Eng. Chem. Res.* **2016**, *56*, 441−456.

(2) Odewunmi, N. A.; Umoren, S. A.; Gasem, Z. M. Watermelon waste products as green corrosion inhibitors for mild steel in HCl solution. *J. Environ. Chem. Eng.* **2015**, *3*, 286−296.

(3) Guo, W.; Chen, S.; Feng, Y.; Yang, C. Investigations of triphenyl phosphate and bis-(2-ethylhexyl) phosphate self-assembled films on iron surface using electrochemical methods, Fourier transform infrared spectroscopy, and molecular simulations. *J. Phys. Chem. C* **2007**, *111*, 3109−3115.

(4) Umoren, S. A. Inhibition of aluminium and mild steel corrosion in acid medium using Gum Arabic. *Cellulose* **2008**, *15*, 751−761.

(5) Banerjee, S.; Srivastava, V.; Singh, M. M. Chemically modified natural polysaccharide as green corrosion inhibitor for mild steel in acidic medium. *Corros. Sci.* **2012**, *59*, 35−41.

(6) Khaladkar, P. R. *Uhlig's Corrosion Handbook*, 2nd ed.; John Wiley & Sons, Inc., 2000; pp 1−1296.

(7) Abboud, Y.; Abourriche, A.; Saffaj, T.; Berrada, M.; Charrouf, M.; Bennamara, A.; Hannache, H. A novel azo dye, 8-quinolinol-5-azoantipyrine as corrosion inhibitor for mild steel in acidic media. *Desalination* **2009**, *237*, 175−189.

(8) Manivel, A.; Ramkumar, S.; Wua, J. J.; Asiri, A. M.; Anandan, S. Exploration of (S)-4,5,6,7-tetrahydrobenzo[d]thiazole-2,6-diamine as feasible corrosion inhibitor for mild steel in acidic media. *J. Environ. Chem. Eng.* **2014**, *2*, 463−470.

(9) Trabanelli, G. Inhibitors − an old remedy for a new challenge. *Corrosion* **1991**, *47*, 410−419.

(10) Ashassi-Sorkhabi, H.; Shaabani, B.; Seifzadeh, D. Corrosion inhibition of mild steel by some Schiff base compounds in hydrochloric acid. *Appl. Surf. Sci.* **2005**, *239*, 154−164.

(11) Solmaz, R. Investigation of the inhibition effect of 5-((E)-4-phenylbuta-1, 3-dienylideneamino)-1, 3, 4-thiadiazole-2-thiol Schiff base on mild steel corrosion in hydrochloric acid. *Corros. Sci.* **2010**, *52*, 3321−3330.

DOI: 10.1021/acsomega.7b00501
ACS Omega 2017, 2, 5691−5707

(12) Oguzie, E. E.; Oguzie, K. L.; Akalezi, C. O.; Udeze, I. O.; Ogbulie, J. N.; Njoku, V. O. Natural products for materials protection: Corrosion and microbial growth inhibition using Capsicum frutescens biomass extracts. *ACS Sustainable Chem. Eng.* **2013**, *1*, 214−225.
(13) Mobin, M.; Aslam, R.; Aslam, J. Non toxic biodegradable cationic gemini surfactants as novel corrosion inhibitor for mild steel in hydrochloric acid medium and synergistic effect of sodium salicylate: experimental and theoretical approach. *Mater. Chem. Phys.* **2017**, *191*, 151−167.
(14) Bouklah, M.; Benchat, N.; Aouniti, A.; Hammouti, B.; Benkaddour, M.; Lagrenee, M.; Vezin, H.; Bentiss, F. Effect of the substitution of an oxygen atom by sulphur in a pyridazinic molecule towards inhibition of corrosion of steel in 0.5 M H_2SO_4 medium. *Prog. Org. Coat.* **2004**, *51*, 118−124.
(15) Mobin, M.; Aslam, R.; Zehra, S.; Ahmad, M. Bio-/environment-friendly cationic gemini surfactant as novel corrosion inhibitor for mild steel in 1 M HCl solution. *J. Surfactants Deterg.* **2017**, *20*, 57−74.
(16) Caroline, M. M.; Christian, P.; Hannes, C. S.; Boris, K.; Ilhan, A. A. Inhibition and promotion of copper corrosion by CTAB in a micro reactor system. *Langmuir* **2008**, *24*, 14269−14275.
(17) El Azhar, M.; Mernari, B.; Traisnel, M.; Bentiss, F.; Lagrenee, M. Corrosion inhibition of mild steel by the new class of inhibitors [2,5-bis(n-pyridyl)-1,3,4-thiadiazoles] in acidic media. *Corros. Sci.* **2001**, *43*, 2229−2238.
(18) Winkler, D. A.; Breedon, M.; Hughes, A. E.; Burden, F. R.; Barnard, A. S.; Harvey, T. G.; Cole, I. Towards chromate-free corrosion inhibitors: structure−property models for organic alternatives. *Green Chem.* **2014**, *16*, 3349−3357.
(19) Ramachandran, S.; Tsai, B.; Blanco, M.; Chen, H.; Tang, Y.; Goddard, W. A. Self-assembled monolayer mechanism for corrosion inhibition of iron by imidazolines. *Langmuir* **1996**, *12*, 6419−6428.
(20) Zhu, Y.; Free, M. L.; Cho, J. H. Integrated evaluation of mixed surfactant distribution in water-oil-steel pipe environments and associated corrosion inhibition efficiency. *Corros. Sci.* **2016**, *110*, 213−227.
(21) Menger, F. M.; Keiper, J. S. Gemini surfactants. *Angew. Chem., Int. Ed.* **2000**, 1906−1920.
(22) Zana, R.; Xia, J. *Gemini Surfactants*; Marcel Dekker: New York, 2004; pp 301−319.
(23) Pérez, L.; Pinazo, A.; Pons, R.; Infante, M. R. Gemini surfactants from natural amino acids. *Adv. Colloid Interface Sci.* **2014**, *205*, 134−155.
(24) Pinazo, A.; Pons, R.; Pérez, L.; Infante, M. R. Amino acids as raw material for bio-compatible surfactants. *Ind. Eng. Chem. Res.* **2011**, *50*, 4805−4817.
(25) Yoshimura, T.; Sakato, A.; Tsuchiya, K.; Ohkubo, T.; Sakai, H.; Abe, M.; Esumi, K. Adsorption and aggregation properties of amino acid-based *N*-alkyl cysteine monomeric and N,N′-dialkylcystine gemini surfactants. *J. Colloid Interface Sci.* **2007**, *308*, 466−473.
(26) Rosen, M. J.; Aronson, S. Standard free energies of adsorption of surfactants at the aqueous solution/air interface from surface tension data in the vicinity of the critical micelle concentration. *Colloids Surf.* **1981**, 3, 201−208.
(27) Al-Sabagh, A. M. Surface activity and thermodynamic properties of water-soluble polyester surfactants based on 1, 3-dicarboxymethoxybenzene used for enhanced oil recovery. *Polym. Adv. Technol.* **2000**, *1*, 48−56.
(28) Sayed, G. H.; Ghuiba, F. M.; Abdou, M. I.; Badr, E. A.; Tawfik, S. M.; Negm, N. A. Synthesis, surface and thermodynamic parameters of some biodegradable nonionic surfactants derived from tannic acid. *Colloids Surf., A* **2012**, *393*, 96−104.
(29) Tawfik, S. M.; Zaky, M. F.; Mohammad, T. G. M.; Attia, H. A. E. Synthesis, characterization, and in vitro antifungal activity of anionic and nonionic surfactants against crop pathogenic fungi. *J. Ind. Eng. Chem.* **2015**, *29*, 163−171.
(30) Haidara, H.; Vonna, L.; Schultz, J. Kinetics and thermodynamics of surfactant adsorption at model interfaces: evidence of structural transitions in the adsorbed films. *Langmuir* **1996**, *12*, 3351−335.
(31) Gibbs, J. W. *The Collected Works of J.W. Gibbs*; Longman, Green and Co.: London, 1928; pp 119−175.
(32) Alsabagh, A. M.; Elsabee, M. Z.; Moustafa, Y. M.; Elfky, A.; Morsi, R. E. Corrosion inhibition efficiency of some hydrophobically modified chitosan surfactants in relation to their surface active properties. *Egypt. J. Pet.* **2014**, *23*, 349−359.
(33) Flores, E. A.; Olivares, O.; Likhanova, N. V.; Domínguez-Aguilar, M. A.; Nava, N.; Guzman-Lucero, D.; Corrales, M. Sodium phthalamates as corrosion inhibitors for carbon steel in aqueous hydrochloric acid solution. *Corros. Sci.* **2011**, *53*, 3899−3913.
(34) Labjar, N.; Lebrini, M.; Bentiss, F.; Chihib, N. E.; El Hajjaji, S.; Jama, C. Corrosion inhibition of carbon steel and antibacterial properties of aminotris-(methylnephosnic) acid. *Mater. Chem. Phys.* **2010**, *119*, 330−336.
(35) Hegazy, M. A.; Abdallah, M.; Awad, M. K.; Rezk, M. Three novel di-quaternary ammonium salts as corrosion inhibitors for API X65 steel pipeline in acidic solution. Part I: experimental results. *Corros. Sci.* **2014**, *81*, 54−64.
(36) Ehteshamzadeh, M.; Jafari, A. H.; Naderi, E.; Hosseini, M. G. Effect of carbon steel microstructures and molecular structure of two new Schiff base compounds on inhibition performance in 1 M HCl solution by EIS. *Mater. Chem. Phys.* **2009**, *113*, 986−993.
(37) Xu, B.; Yang, W.; Liu, Y.; Yin, X.; Gong, W.; Chen, Y. Experimental and theoretical evaluation of two pyridinecarboxaldehydethiosemicarbazone compounds as corrosion inhibitors for mild steel in hydrochloric acid solution. *Corros. Sci.* **2014**, *78*, 260−268.
(38) Daoud, D.; Douadi, T.; Hamani, H.; Chafaa, S.; Al-Noaimi, M. Corrosion inhibition of mild steel by two new S-heterocyclic compounds in 1 M HCl: Experimental and computational study. *Corros. Sci.* **2015**, *94*, 21−37.
(39) Shaban, S. M.; Aiad, I.; El-Sukkary, M. M.; Soliman, E. A.; El-Awady, M. Y. Inhibition of mild steel corrosion in acidic medium by vanillin cationic surfactants. *J. Mol. Liq.* **2015**, *203*, 20−28.
(40) Al-Sabagh, A. M.; Nasser, N. M.; El-Azabawy, O. E.; El-Tabey, A. E. Corrosion inhibition behavior of new synthesized nonionic surfactants based on amino acid on carbon steel in acid media. *J. Mol. Liq.* **2016**, *219*, 1078−1088.
(41) Shaban, S. M.; Abd-Elaal, A. A.; Tawfik, S. M. Gravimetric and electrochemical evaluation of three nonionic dithiol surfactants as corrosion inhibitors for mild steel in 1 M HCl solution. *J. Mol. Liq.* **2016**, *216*, 392−400.
(42) Hegazy, M. A.; Abd El Rehim, S. S.; Badawi, A. M.; Ahmed, M. Y. Studying the corrosion inhibition of carbon steel in hydrochloric acid solution by 1-dodecyl-methyl-1Hbenzo[d][1,2,3]triazole-1-ium bromide. *RSC Adv.* **2015**, *5*, 49070−49079.
(43) Badawi, A. M.; Hegazy, M. A.; El-Sawy, A. A.; Ahmed, H. M.; Kamela, W. M. Novel quaternary ammonium hydroxide cationic surfactants as corrosion inhibitors for carbon steel and as biocides for sulfate reducing bacteria (SRB). *Mater. Chem. Phys.* **2010**, *124*, 458−465.
(44) Shaban, S. M.; Aiad, I.; El-Sukkary, M. M.; Soliman, E. A.; El-Awady, M. Y. Inhibition of mild steel corrosion in acidic medium by vanillin cationic surfactants. *J. Mol. Liq.* **2015**, *203*, 20−28.
(45) Hegazy, M. A.; El-Tabei, A. S.; Bedair, A. H.; Sadeq, M. A. Synthesis and inhibitive performance of novel cationic and gemini surfactants on carbon steel corrosion in 0.5 M H_2SO_4 solution. *RSC Adv.* **2015**, *5*, 64633−64650.
(46) Qiu, L. G.; Xie, A. J.; Shen, Y. H. Understanding the adsorption of cationic gemini surfactants on steel surface in hydrochloric acid. *Mater. Chem. Phys.* **2004**, *87*, 237−240.
(47) Qiu, L. G.; Xie, A. J.; Shen, Y. H. A novel triazole-based cationic gemini surfactant: synthesis and effect on corrosion inhibition of carbon steel in hydrochloric acid. *Mater. Chem. Phys.* **2005**, *91*, 269−273.
(48) Abd El-Lateef, H. M.; Soliman, K. A.; Tantawy, A. H. Novel synthesized Schiff base-based cationic gemini surfactants: electrochemical investigation, theoretical modeling and applicability as biodegradable inhibitors for mild steel against acidic corrosion. *J. Mol. Liq.* **2017**, *232*, 478−498.
(49) Jeeva, M.; Prabhu, G. V.; Boobalan, M. S.; Rajesh, C. M. Interactions and inhibition effect of urea-derived mannich bases on mild steel surface in HCl. *J. Phys. Chem. C* **2015**, *119*, 22025−22043.

DOI: 10.1021/acsomega.7b00501
ACS Omega 2017, 2, 5691−5707

(50) Ekanem, U. F.; Umoren, S. A.; Udousoro, I. I.; Udoh, A. P. Inhibition of Mild Steel Corrosion in HCl Using Pineapple Leaves-(Ananas Comosus L.) Extract. *J. Mater. Sci.* **2010**, *45*, 5558−5566.
(51) Yadav, M.; Kumar, S.; Sinha, R. R.; Behera, D. Experimental and quantum chemical studies on corrosion inhibition performance of Benzimidazole derivatives for mild steel in HCl. *Ind. Eng. Chem. Res.* **2013**, *52*, 6318−6328.
(52) Saleh, M. M.; Atia, A. A. Effects of structure of the ionic head of cationic surfactant on its inhibition of acid corrosion of mild steel. *J. Appl. Electrochem.* **2006**, *36*, 899−905.
(53) Martinez, S.; Stern, I. Thermodynamic characterization of metal dissolution and inhibitor adsorption processes in the low carbon steel/mimosa tannin/sulfuric acid system. *Appl. Surf. Sci.* **2002**, *199*, 83−89.
(54) Loganayagi, C.; Kamal, C.; Sethuraman, M. G. Opuntiol: An active principle of Opuntiaelatior as an eco-Friendly inhibitor of corrosion of mild steel in acid medium. *ACS Sustainable Chem. Eng.* **2014**, *2*, 606−613.
(55) Obot, I. B.; Ebenso, E. E.; Kabanda, M. M. Metronidazole as environmentally safe corrosion inhibitor for mild steel in 0.5 M HCl: Experimental and theoretical investigation. *J. Environ. Chem. Eng.* **2013**, *1*, 431−439.
(56) Obot, I. B.; Umoren, S. A.; Gasem, Z. M.; Suleiman, R.; El-Ali, B. Theoretical prediction and electrochemical evaluation of vinylimidazole and allylimidazole as possible green corrosion inhibitors for carbon steel in 1 M HCl. *J. Ind. Eng. Chem.* **2015**, *21*, 1328−1339.
(57) Solmaz, R.; Kardas, G.; Yazici, B.; Erbil, M. Adsorption and corrosion inhibitive properties of 2-amino-5-mercapto-1,3,4-thiadiazole on mild steel in hydrochloric acid media. *Colloids Surf., A* **2008**, *312*, 7−17.
(58) Abd El-Lateef, H. M.; Tantawy, A. H. Synthesis and evaluation of novel series of Schiff base cationic surfactants as corrosion inhibitors for carbon steel in acidic/chloride media: experimental and theoretical investigations. *RSC Adv.* **2016**, *6*, 8681−8700.
(59) Mobin, M.; Zehra, S.; Aslam, R. L-Phenylalanine methyl ester hydrochloride as a green corrosion inhibitor for mild steel in hydrochloric acid solution and the effect of surfactant additive. *RSC Adv.* **2016**, *6*, 5890−5902.
(60) Parveen, M.; Mobin, M.; Zehra, S. Evaluation of L-tyrosine mixed with sodium dodecyl sulphate or cetyl pyridinium chloride as a corrosion inhibitor for mild steel in 1 M HCl: experimental and theoretical studies. *RSC Adv.* **2016**, *6*, 61235−61248.
(61) Kumar, A. M.; Babu, R. S.; Obot, I. B.; Gasem, Z. M. Fabrication of nitrogen doped graphene oxide coatings: experimental and theoretical approach for surface protection. *RSC Adv.* **2015**, *5*, 19264−19272.
(62) Yuce, A. O.; Kardas, G. Adsorption and inhibition effect of 2-thiohydantoin on mild steel corrosion in 0.1 M HCl. *Corros Sci.* **2012**, *58*, 86−94.
(63) Badawy, W. A.; Ismail, K. M.; Fathi, A. M. Environmentally safe corrosion inhibition of the Cu−Ni alloys in acidic sulfate solutions. *J. Appl. Electrochem.* **2005**, *35*, 879−888.
(64) Oguzie, E. E.; Li, Y.; Wang, F. H. Corrosion inhibition and adsorption behavior of methionine on mild steel in sulfuric acid and synergistic effect of iodide ion. *J. Colloid Interface Sci.* **2007**, *310*, 90−98.

DOI: 10.1021/acsomega.7b00501
ACS Omega 2017, 2, 5691−5707